A novel Long-noncoding RNA LncZFAS1 prevents MPP$^+$-induced neuroinflammation through MIB1 activation

Ziman Zhu
Capital Medical University
Peiling Huang
Capital Medical University
Ruifeng Sun
Capital Medical University
Xiaoling Li
Capital Medical University
Wenshan Li
Capital Medical University
Weijun Gong (gwj197104@ccmu.edu.cn)
Capital Medical University

Research Article

Keywords: LncZFAS, Parkinson's disease, pyroptosis, MIB1, TXNIP, NLRP3

Posted Date: August 2nd, 2021

DOI: https://doi.org/10.21203/rs.3.rs-770278/v1

Version of Record: A version of this preprint was published at Molecular Neurobiology on November 13th, 2021. See the published version at https://doi.org/10.1007/s12035-021-02619-z.

Abstract

Parkinson's disease remains one of the leading neurodegenerative diseases in developed countries. Despite well-defined symptomology and pathology, the complexity of Parkinson's disease prevents a full understanding of its' etiological mechanism. Mechanistically, α-synuclein misfolding and aggregation appears central for disease progression, but mitochondrial dysfunction, dysfunctional protein clearance and ubiquitin/proteasome systems, and neuroinflammation have also been associated with Parkinson's disease. Particularly neuroinflammation, which was initially thought to be a side effect of Parkinson's disease pathogenesis, has now been recognized as driver of Parkinson's disease exacerbation. Next-generation sequencing identified a plethora of long noncoding RNAs (lncRNA) with important transcriptional regulatory functions. Moreover, a myriad of lncRNA are known regulators of inflammatory signaling and neurodegenerative diseases including IL-1β secretion and Parkinson's disease. Here lncZFAS1 was identified as a regulator of inflammasome activation and pyroptosis in human neuroblast SH-SY5Y cells following MPP^+ treatment, a common *in vitro* Parkinson's disease cell model. Mechanistically, TXNIP ubiquitination through MIB1 E3 ubiquitin ligase regulates NLRP3 inflammasome activation in neuroblast cells. In contrast MPP^+ activates the NLPR3 inflammasome through miR590-3p up-regulation, and direct interference with MIB1-dependent TXNIP ubiquitination. LncZFAS overexpression inhibits this entire pathway through direct interference with miR590-3p exposing a novel therapeutic target to prevent excessive inflammasome activation and pyroptosis in neuroblast cells during Parkinson's disease.

Introduction

Parkinson's disease (PD) is one of the leading neurodegenerative diseases in developed countries, afflicting 1-2% of elderly population (over 65 years old)[1]. The world health organization predicts that PD incidence will double by 2030[2] with significant loss of healthy life years. PD syndrome is defined by tremor, rigidity, progressive akinesia and/or postural disturbance. PD is a multifactorial disease associated with both genetic and environmental factors, but a complete etiological scenario is still unknown. Nonetheless, PD pathology is well defined and primarily characterized by the loss of dopaminergic neurons in the substantia nigra[3]. Mechanistically, α-synuclein misfolding and aggregation seems central for disease progression, but mitochondrial dysfunction, dysfunctional protein clearance and ubiquitin/proteasome systems, and neuroinflammation have also been connected with PD disease.

Without a well-defined etiological model, development and identification of novel therapeutic target must rely on high throughput screening in immortalized or primary neural cell lines[4]. SH-SY5Y human neuroblast cells are commonly used as an alternative to laborious and highly heterogeneous primary dopaminergic neuron cultures from rat/mouse embryos[5, 6]. Regardless of the cell model, 1-methyl-4-phenylpyridinium (MPP^+) is generally used to induce PD-like cellular disease. MPP^+ is a dopaminergic neurotoxin, and the active metabolite of MPT (1-methyl-4-phenyl-1,2,3,6-tetrahydropyridine), that is known to cause human parkinsonism after injection[7].

Neuroinflammation was initially thought to be a side effect of PD pathogenesis. This perspective has since then been revised and microglial inflammatory signals are now known to exacerbate and significantly contribute for PD progression[8-11]. Inflammasomes sense microbial infection or host-derived danger signals indicative of metabolic perturbations[12]. These large multimeric Caspase1-activating complexes control maturation and secretion of interleukins such as IL-1b and IL-18 with potent proinflammatory activities against infection and injury[12, 13]. Many inflammasome are activated through direct interaction with pathogen- or danger- associated molecular patters (PAMPS and DAMPS) [12]. Nod-like receptor with pyrin domain (NLRP) 3, however, can sense intracellular metabolic perturbations, such intracellular ATP and K^+ ion imbalance or oxidative stress through yet unclear mechanisms[14]. Perhaps for this reason, NLRP3 has been extensively associated with autoimmune disease and chronic inflammation[15, 16]. Furthermore, MPTP-driven NLRP3 inflammasome activation in microglia has been recently shown to play a central role in dopaminergic neurodegeneration and PD[17]. NLRP3 is regulated by both transcriptional, post-transcriptional and post-translational signals[18]. In homeostasis, NLRP3 is general expressed in extremely low levels, but quickly and highly up-regulated after PAMP or DAMP prime singling[19]. In the cytosol, NLRP3 senses K^+ efflux, intracellular oxidative stress or extracellular elevated ATP levels[19]. Any of these metabolic perturbations induce NLRP3 oligomerization, interaction with the adaptor protein ASC and recruitment of cysteine protease pro-caspase-1[5]. Autocatalysis and activation of caspase-1 lead to cleavage, maturation and secretion of proinflammatory cytokines IL-1β and IL-18 and, sometimes, to induction of programmed inflammatory cell death by pyroptosis[20-23].

The next-generation sequencing revolution identified a plethora of long noncoding RNAs (lncRNA), previously assumed as biologically irrelevant, but now known to have important transcriptional regulatory functions[24]. Recently lncRNAs have also been shown to regulate protein expression post-transcriptionally through interference with microRNAs (miRs), smaller nonconding RNAs that directly bind to protein-coding mRNA, inhibiting translation and promoting transcript degradation[25, 26]. Moreover, a myriad of lncRNA and miR have been linked to regulation of inflammatory signaling and neurodegenerative diseases including IL-1β secretion and PD[27, 28].

ZNFX1 antisense RNA 1 (ZFAS1), was recently identified as a novel lncRNA transcribed from the antisense orientation of zinc finger NFX1-type containing 1(ZNFX1) located on chromosome 20q13.13[29]. Over the past 5 years, lncZFAS1 emerged as regulatory factor in multiple diseases, such as acute myocardial infarction[30, 31], rheumatoid arthritis[32], and cancer[33]. Interestingly, much like PD, myocardial infarction and rheumatoid arthritis are also driven and exacerbated by dysregulated inflammasome activation[34]. Furthermore, lncZFAS1 shows a broad molecular functional profile interfering in complex pathways including cell proliferation and cell death[35]. Therefore, despite not being previously associated with PD, we hypothesized that lncZFAS1 might regulate inflammasome activation and pyroptosis during PD. Here lncZFAS1 was identified as a regulator of inflammasome activation and pyroptosis in human neuroblast SH-SY5Y cells following MPP^+ treatment. This work

unveils a potential beneficial role of lncZFAS1 during PD progression, which can be explored as a new therapeutic target.

Materials And Methods

Tissue culture

SH-SY5Y cell were acquired from ATCC and maintained in DMEM/F12 (1:1) with penicillin (100 U/mL), streptomycin (100 µg/mL) and 10% FBS. At 90% confluency, monolayer was washed twice with PBS, and cells chemically detached with 0.05% trypsin for 2 min. After quenching with complete media, cells were pelleted by centrifugation at 800 rpm for 5 minutes, washed twice with PBS, resuspended in complete medium and $3x10^4$ to 10^6 cells seeded in 10cm tissue culture dishes. Medium was changed every other day. SH-SY5Y cells were differentiated into dopaminergic neuron-like cells with (10 µM) retinoic acid in DMEM (1%FBS) for 5 days. Upon differentiation, cell adherence was confirmed under the microscope, and leftover suspension cells were removed by gentle washing.

Pyroptosis assay

SH-SY5Y cells were seeded in 6-well plates at 10^6 cells/well for 24 hours and then treated with increasing MPP^+ concentrations for 24 hours. Cells were the gently washed with PBS and chemically detached with 0.05% trypsin/EDTA. After detachment, trypsin was quenched with complete media, cells pelleted by centrifugation and caspase activity detected with FAM-FLICA capase-1 assay kit (ImmunoChemistry Technologies, LLC, Bloomington, MN, USA) according to manufacturer's recommendations. In a nutshell, cells were stained were incubated with FLICA (1:30) for 1 hour at 37°C protected from light. Cells were then by washed with 5 volumes of 1X apoptosis wash buffer, pelleted by centrifugation, resuspended in 1X apoptosis wash buffer with 5µL of PI and incubated for 10 minutes 37°C protected from light. Data was acquired with Beckman DxFlex flow cytometer (Beckman, USA) and analyzed with CytExpert (Beckman Coulter Inc, CA, USA). Single stain controls were used to calculate compensation. PI positive cells were detected according to the operation procedure of PI staining kit (KeyGEN Biotech, NanJing, China)

Total protein extraction

Cells were seeded in 6-well plates at 10^6 cells/well and treated with 1mM MPP^+. When designated, cells were also treated with mir590-3p mimic or inhibitor and corresponding negative controls. At designated timepoints, cells were washed with pre-cooled PBS and lysed with 1 ml of RIPA buffer supplemented with PMSF for each 100 µL of sample. After full lysis, samples were centrifuged at 12,000 g, 4 ℃ for 5 min, the supernatant immediately transferred to a clean pre-cooled tube and stored at -80 ℃ for later analysis. Total protein content was quantified by BCA method, 25µg added to 5×loading buffer and boiled for 10 minutes in water bath for denaturing. Samples were stored at -20 ℃ until western blot analysis when needed.

Immunoprecipitation (Co-IP) assay

Protein extracts were prepared as described above. Protein A/G-agarose microspheres were washed twice with PBS and adjusted to a 50% agarose microspheres concentration in PBS. In detail, 100 μL of 50% of Protein A/G-agarose were added to 1mL of sample and incubated in a horizontal shaker at 4°C for 10 min to remove unspecific binding. Samples were then centrifuge at 14000 g for 15 minutes at 4°C, and the supernatant transferred to a clean centrifuge tube. Total protein was estimated by BCA method, and adjusted to 3 μg/μL with PBS. Immunoprecipitation microspheres were prepared in 500μL with pre-titrated target antibody and 1 volume of bead mixed with 7 volumes of sample. Samples were incubated overnight at 4℃ with gentle shaking, centrifuged at 14000g for 5s, the precipitate collected, and washed 3 times with pre-cooled washing buffer (800μL per wash). The pellet was resuspended in a suitable volume of loading buffer and the supernatant collected for further downstream SDS-PAGE western-blot analysis.

Western blotting

Denatured samples were loaded in 10% or 12% resolving and 5% stacking SDS-PAGE gels prepared in house. Denatured samples were separated by electrophoresis in the MINI-PTET (BioRad, California, USA) system at 120 V for 5 min (stacking) and 80 V (resolving) for about 30 min with pre-chilled 1× electrophoresis buffer. 5 μL of 3-color pre-stained protein ladder (Green, BioReseach LLC, LA, USA) was used as standard for protein size estimation. For transfer, PVDF membrane was pre-activated in methanol for 1 min, and then immersed in the transfer buffer for 15 minutes. Samples were transferred with semi-dry blot apparatus (BioRad, California, USA). Transfer efficiency was confirmed by Ponceau S staining. For specific protein expression, membranes were incubated with primary antibody, at pre-titrated concentrations (Table 1), in Tris buffered saline/0.05%Tween20 (TBST) and self-sealing bags and incubated overnight at 4℃. Membranes were then washed three time with TBST for 10 min with gentle rocking, and antibody binding detected with appropriate HRP-conjugated secondary antibody at pre-titrated concentrations in Ziplock bags for 1 hour at room temperature. Membranes were washed again 3 times with TBST. Membranes were developed with ECL Luminescent Solution (Thermo Fisher Scientific, Pittsburgh, PA, USA) for 5 min according to manufactures' instructions. Membranes were imaged with Tanon 6600 Luminescent imaging workstation (Tanon, Shanghai, China) and relative protein expression levels quantified with Image Pro Plus 6.0 software (Media Cybernetics, USA). The expression level was calculated as [target protein gray value]/[internal reference protein gray value].

RNA extraction

SH-SY5Y cells were seeded in 6-well plates at 10^6 cells/well and treated with MPP^+ as described above. At 90% confluency or designated timepoints cells were chemically detached with trypsin, lysed with RNAiso plus Trizol, at room temperature for 10min and RNA extracted according to manufacturers' recommendations. In a nutshell, 1/5 volume of chloroform was added, samples were shaken and let stand at room temperature for 5min, followed by 15 minutes centrifugation at 12000g 4°C. Supernatants

were transferred to a clean centrifuge tube, 1 volume of isopropanol added, and the samples inverted and mixed vigorously. After 10 minutes incubation on ice, samples were centrifuged at 12000g, 4°C for 10min and the supernatant discarded. RNA was washed with 1ml of 75% ethanol, air-dried (5-10 min) and resuspended in 20 µl of RNase-free water. RNA content, purity and quality were estimated with Nanodrop 2000 (Thermo fisher, USA) (2µL of sample).

MicroRNA extraction

SH-SY5Y cells were seeded in 6-well plates at 10^6 cells/well and treated with MPP^+ as described above. At 90% confluency (unless otherwise stated), cells were chemically detached with trypsin, pelleted by centrifugation and resuspended in 100µL of PBS. MiRNA was extracted with tissue/cell miRNA extraction kit (Haigene, Harbin, China) according to manufacturers' recommendations. In a nutshell, 300 µL of miRNA ReagentA were added, the sample mixed by inversion and incubated at room temperature for 5 min. After lysis, 250 µL of miRNA ReagentB was added, again mixed by inversion and centrifuged at 13000rpm for 5 min. The supernatant was transferred to a clean 1.5 ml tube, 200 µL of absolute ethanol added, mixed vigorously, and incubated at room temperature for 5 min with shaking. After centrifugation at 13000 rpm for 10 min, isopropanol was added (3:7 volume ratio), the sample inverted several times and loaded into the miRNA adsorption column. Column was washed twice with 75% absolute ethanol, dried for 10 min and eluted with 30 µL RnaseFree TE Buffer to a new clean tube by centrifugation at 13000rpm for 2 min.

qRT-PCR

First strand cDNA reverse transcription from mRNA was performed with iScript cDNA synthesis Kit (BioRad, USA) according to manufacturers' recommendations in 20µL reactions with 2µL of total RNA. The reaction was performed at 25°C for 5 min, 42°C for 30 min, and 85°C for 5 min, and cDNA stored at -70°C. qRT-PCR was performed with Sofast EvaGreen Supermix system (BioRad, USA) in 20µL reactions with 1µL cDNA template according to manufacturer's recommendations in a ABI 7500 real-time quantitative PCR instrument (American Applied Biosystems, USA).

First strand cDNA reverse transcription from miR and lncRNA was performed with one-step miR RT kit (Takara, Japan) in 20µL reactions with 4µL of RNA template according to manufacturer's recommendations. The reaction was performed for 60 minutes at 37°C, followed by 5 minutes at 95°C. qRT-PCR was performed with cDNA SYBR Green miRNA fluorescence quantitative PCR kit (Haigene, Harbin, China) in 20µL reactions with 2.5µL template cDNA. qRT-PCR was run in ABI 7500 real-time quantitative PCR instrument (American Applied Biosystems, USA). qRT-PCR protocols are shown in table 2. Gene-target specific primers are shown in table 3. Fold change differences in gene expression were calculated by $2^{-\Delta\Delta Ct}$ method.

Lentiviral production

RNAi sequences were cloned into GV493 plasmid and expanded in *E.coli* DH5α cells in house (Fig. S1). LncZFAS1 RNA sequence was cloned into pcDNA3.1 (Fig. S2). Lentiviral packaging was performed in 293T cells seeded at 5×10^6 cells/15mL in T75 flask in DMEM medium with 10% FBS for 24 before transfection. At 70-80% confluency, cells were washed with PBS, 1 volume of serum-free medium added and incubated for 2 hours incubation at 37°C 5% CO_2 . Transfection mixture was prepared with 20 µL of vector plasmid, mixed with 15 µL pHelper1.0 vector plasmid, 10 µL pHelper 2.0 vector plasmid, and GK transfection reagent (Genechem, Shanghai, China), in a total 1mL volume reaction, and incubated at room temperature for 15 min. The transfection mixture was slowly added to the 293T cell culture (in serum-free medium) with gentle rocking, and incubated at 37°C, 5% CO2 for 6 hours. Cells were gently washed with warm PBS, 20mL of complete medium (with 10% FBS) added and incubated at 37°C and 5% CO_2 for 48 h. Supernatants were collected 48 h after transfection, centrifuged at 4000 g for 10 min at 4°C to remove cell debris and transferred to 40 ml ultra-centrifuge tubes through 0.45 µm filter. Lentiviral particles were pelleted by ultracentrifugation at 25000 rpm, 4°C for 2 h, media supernatant was discarded, lentiviral particles resuspended in residual volume and transferred to clean tube. Samples were centrifuged one last time, at 10,000 rpm for 5 minutes and the supernatant containing lentiviral particles transferred to a clean tube. Lentivirus titer was detected in 293T adherent cells. Cells were seeded in 96 well-plates at 4×104 cells/well, in 100 µL medium and incubated for 24 hours. Lentiviral preps were serial diluted (1/10) in serum free media (10 to 10^{-10}), added to T293 cells and incubated at 37°C and 5% CO_2 for 24 hours. 100 µL of complete medium was added and lentiviral titer measured after 4 days by fluorescence expression. Lentiviral titer was determined as transducing units (TU/ml) calculated as **see formula 1 in the supplementary files section** .

Lentivirus transfection

SH-SY5Y cells were seeded in 24-well plates at 0.5×10^5 cells/well and incubated at 37°C, 5% CO_2 overnight. Prior to transfection, cells were washed with PBS, and 500µL of 0.8µg/mL Polybrene in serum-free medium with 20µL lentivirus at pre-titrated MOI of 5 were added. Cells were incubated overnight at 37°C and 5% CO_2, the medium removed and replaced for 1ml of complete medium, and incubated at 37°C and 5% CO^2. Transfected cells were expanded and subcultured at a 1:3 ratio. 48 hours after subculture, cells were seeded in a Petri dishes 200 µg/mL Puromycin selection medium, changed every 3/4 days, until clonal cell clusters appeared. Single cell clones were digested, transferred to 6-well plates, expanded, frozen and stored in liquid nitrogen. Transfection efficiency was confirmed by WB and qRT-PCR (Fig. S3)

Luciferase reporter assay (pMIR-REPORT fluorescent reporter gene)

The 3'UTR full length of the pre-selected target gene MIB1 was identified based on TargetScan Human 7.2 website (http:www.targetscan.org/vert_72/). Primer 5 (Premier, California) was used to design primers (Table 3) with the 3'UTR fragment of the MIB1 gene containing the hsa-miR-590-3p binding site. The MIB1 sequence (with 3'UTR) was then cloned in house into the pmiR-report plasmid (Ambion, Texas, USA, Fig. S4) and expanded in E. coli DH5α cells. First strand cDNA reverse transcription from mRNA was

performed with iScript cDNA synthesis Kit (BioRad, USA) as described above. Site directed mutagenesis was performed with QuickMutagenesis Kit (Thermo Fisher Scientific, Pittsburgh, PA, USA) according to manufacturer's recommendations. SH-SY5Y cells at 50% confluency, were then transfected in 96-well plates with Lipofectamine 3000 system (Thermo Fisher Scientific, Pittsburgh, PA, USA) according to manufacturer's recommendations. Luciferase double reporter gene expression was detected with dual luciferase reporter gene detection kit (KeyGEN Biotech, NanJing, China) according to manufacturer's recommendations. Briefly, after 36-48h of plasmid co-transfection, medium was discarded, and the cells washed with 100μL 1X PBS. 50 μL of 1X PLB was added to each well, and the plate incubated for 20-30 min with shaking to ensure lysis. 10μL of the supernatant were added to 96-well white opaque microtiter plate (Thermo fisher, USA), followed by 100μL of pre-mixed Luciferase Assay Reagent II. Plates were read in a dark chamber with a Berthold LB941 microplate multi-functional microplate reader (Berthold, Germany) 2s after starting reaction to detect the luciferase activity (RLU1). 100 μL of pre-mixed Stop&Glo Reagent were then added to each well to detect the intensity of the luciferase reaction in the internal reference control (RLU2). Gene-specific luciferase activity was calculated as RLU1/RLU2.

miR590-3p mimic and inhibition assay

hsa-miR-590-3p mimics (Sequence: UAAUUUAUGUAUAAGCUAGU), mimic NC (sequence: UUGUACUACACAAAAGUACUG), hsa-miR-590-3p inhibitor (sequence: ACUAGCUUAUA CAUAAAAUUA), Inhibitor-NC (sequence: CAGUACUUUUGUGUAGUACAA) particles were purchased from Nanjing Darn Pharmaceutical Technology Co., Ltd (Nanjing, China). SH-SY5Y cells at 50% confluency were transfected in 6-well plates with Lipofectamine RNAiMAX (Thermo fisher, USA). In detail Lipofectamine RNAiMAX (6μL), 20pmol RNAi were mixed in 200μL OPTI-MEM medium and incubated at room temperature for 20 minutes prior to transfection. SH-SY5Y cells were gently washed with 1×PBS three times, 2 mL of OPTI-MEM medium added to each well, and acclimated to 37 ℃, 5% CO2. Transfection reagent mixture was added to the culture, with gentle shaking and incubated at 37 ℃, 5% CO_2 for 48 hours.

Fluorescent *in situ* hybridization (FISH) and confocal microscopy

FISH staining kit was purchased from RiboBio (Guangzhou, China). Digoxin labeled probes (TACTTCCAACACCCGCATTCATC) were acquire from RiboBio (Guangzhou, China). $2X10^5$ cells SH-SY5Y cells were seeded in 24-well microscopy slides (Thermo Fisher Scientific, Pittsburgh, PA, USA). After treatment, cells were washed with pre-cooled PBS, and fixed with 4% RNase-free Paraformaldehyde at room temperature for 15 minutes. After washing with PBS 3 times for 5 min, cells were permeabilized with 0.2-0.5% Triton X-100 for 5 minutes at room temperature. Cells were washed again with PBS (3×5min) and dehydrated (80%-90%-100% alcohol gradient for 2-3min each). The hybridization solution was prepared in house with Formamide mixed with 2X saline-sodium citrate (SSC) in a 1:1 volume at room temperature for 10 minutes. Cells were washed again with PBS, 25μl of hybridization solution added to each well, and incubated in the hybridization furnace at 50℃ for 4-8h. 60 μl of denaturing hybridization solution containing probe were then added to each well and incubated overnight in the hybridization furnace at 50℃. Cells were wash with 0.1×SSC with 0.1% SDS and 50% formamide for 30

mins. Samples were then blocked with 90 µl 20% sheep serum at room temperature for 1h. Hybridization was detected with 60 µl anti-digoxin antibody, prepared 1/2500 in 10% sheep serum and incubated overnight at 4°C. After washing with PBS, samples were counterstained with add 10 µl of 200 mg/ml DAPI at room temperature for 10 min. Cells were washed one more time with PBS, mounted with 10µl of anti-quenching mounting agent, seal with rubber cement, and imaged with Zeiss LSM laser confocal microscope (Zeiss, Germany).

Statistics and data analysis

All data are expressed as means ± SD. One-way ANOVA and non-parametric Kurskal-Wallis test are used for statistical differences between groups. P-values less than 0.05 are considered significant differences. Data was analysed with Graphpad 6.0 (San Diengo, CA, USA).

Results

MPP^+ induces pyroptosis through inflammasome activation in SH-SY5Y neuronal cells

NLRP3 inflammasome activation and pyroptosis in primary microglial cells is pivotal for MTPT-induced Parkinson's disease progression in murine model[17]. To assess if MPP^+ can also induce inflammasome activation and pyroptosis in a human neuroblast cells, SH-SY5Y cells were treated with MPP^+ increasing concentrations and the frequency of pyroptotic cells was quantified by the internalization of propidium iodide and caspase-1 activation. As expected MPP^+ treatment significantly increases the frequency of pyroptotic SH-SY5Ycells, 24 hours after treatment, from 250nM to 1mM concentrations (Fig. 1A and B). Furthermore MPP^+ treatment significantly induces NLPR3/ASC association, and cleavage of Gsdmd, pro-IL-1β and caspase1, hallmarks of inflammasome activation. MPP^+ had no impact on the protein levels of Gsdmd, pro-IL-1β and caspase1 pre-cleaved peptides (Fig. 1C and D).

LncZFAS1 inhibits MPP^+ induced pyroptosis in SH-SY5Y human neuroblast cells

MicroRNA and LncRNA regulate a myriad of metabolic and inflammatory pathways, including inflammasome activation[24]. LncZFAS role in inflammasome and pyroptosis has not been addressed. To understand the impact of ZFAS in MPP^+ induced pyroptosis this LncRNA was stably transfected in SH-SY5Y cells prior to MMP^+ treatment (Fig. S3). LncZFAS1 over-expressing (oe-lncZFAS1) cells show significantly lower cleavage of Gsdmd, pro-IL-1β and caspase1 following MPP^+ treatment compared to empty vector transfected control cells (oe-Vector), despite no impact in overall pre-cleaved peptide levels (Fig. 2 A-G). Moreover, oe-LncZFAS1 cells have lower NRLP3/ASC association than oe-vector cells 24 h after MPP^+ treatment (Fig. 2H). Consequently, oe-LncZFAS1 SH-SY5Y cells are resistant to MPP^+-induced pyroptosis (Fig. 2 I-K).

To confirm the role of LncZFAS on MMP^+ induced pyroptosis, this LncRNA was stably knocked-out in SH-SY5Y cells (sgRNA-ZFAS1) (Fig. 3). MPP^+ treated sgRNA-ZFAS1 cells show significantly higher cleavage

of Gsdmd, pro-IL-1β and caspase1 then MPP^+ treated control cells, despite no impact in overall pre-cleaved peptide levels (Fig. 3 A-G). Additionally, sgRNA-ZFAS1 cells have higher NRLP3/ASC association than sgRNA-NC cells 24 h after MPP^+ treatment (Fig. 3H). Finally, sgRNA-ZFAS1 cells showed higher sensitivity to MPP^+-induced pyroptosis (Fig. 3I-K).

LncZFAS1 blocks MPP+ induced oxidative stress through TRX1/TXNIP redox signaling complex

Increased intracellular oxidative stress can act as second signal for NLRP3 inflammasome activation[18, 21-23]. To assess if MPP^+ induces intracellular oxidative stress SH-SY5Y cells, intracellular ROS was measured with DCFH-DA ROS-sensing fluorescent probe and analyzed by flow cytometry. As expected MPP^+ significantly induces intracellular ROS in SH-SY5Y human neuroblast cells 24 hours after treatment (Fig. 4A and B). Furthermore, to understand if LncZFAS1 inhibits MPP^+-induced oxidative stress, oe-SHSY5Y cells were treated with MPP^+ and intracellular ROS-levels measure 24 hours after treatment. Again, as hypothesized, LncZFAS1 over-expression significantly decreases intracellular oxidative stress compared to corresponding empty vector transfected control cells (Fig. 4A and B).

Increased oxidative stress activate NLRP3 inflammasome through induction and activation of TXNIP redox-sensing complex, but a defined molecular mechanism remains elusive[36, 37]. In SH-SY5Y cells MPP^+ does not change TXNIP protein transcriptional and translational levels (Fig. 4C-E), neither TXNIP/TRX1 interaction (Fig. 4F). In contrast, LncZFAS1 significantly decreases post-translational TXNIP protein levels (Fig. 4C-E) with a prominent decrease in TXNIP/TRX1 interaction (Fig. 4F).

Again, to further validate the impact of LncZFAS1 TXNIP redox-sensing complex in response to MPP+, the expression levels of TXNIP/TRX1 were measured in sgRNA-ZFAS1 cells. As expected LncZFAS1 knockout significantly increased TXNIP protein levels, without impacting transcriptional levels (Fig. 5A, B and D). Moreover, after immunoprecipitation with an anti-TXNIP antibody, MPP^+-treated sgRNA-ZFAS1 cells show increased interaction with TRX1 compared to sgRNA-NC cells, which is likely due to increased TXNIP protein levels (Fig. 5C). Finally, to confirm that LncZFAS1 regulates intracellular oxidative stress response to MPP^+, ROS levels were measured in sgRNA-ZFAS1 and corresponding sgRNA-NC cells 24 hours after MPP^+ stimulation. In accordance with our previous observations LncZFAS1 knockout significantly induces intracellular ROS production following MPP+ stimulation in SH-SY5Y cells (Fig. 5E and F).

LncZFAS1 inhibits inflammasome activation through TXNIP proteasomal degradation

The proteasomal degradation pathway has been recently identified as a major regulator of inflammasome activation[38]. To assess if LncZFAS1 post-translationally downregulates TXNIP through proteasome degradation pathway oe-ZFAS1 cells were treated with MPP^+ and MG132 proteasome inhibitor. As expected, proteasomal inhibition rescued TXNIP protein levels and TXNIP/TRX1 interactions in oe-ZFAS SY-SH5Y neuroblast cells (Fig. 6A, B, D and E). Consistent with the role of TXNIP in NLRP3 inflammasome activation, proteasomal inhibition rescued cleavage of Gsdmd, pro-IL-1β and caspase1 (Fig. 6C, F, H, J), hallmarks of inflammasome activation in oe-ZFAS SY-SH5Y cells following MPP^+

treatment. Proteasome inhibition had no impact on the protein levels of Gsdmd, pro-IL-1β and caspase1 pre-cleaved peptides (Fig. 6C, G, I). Once gain the exact opposite was observed after LNCZFAS1 knockout (Fig. 7). sgRNA-ZFAS1 cells show increased TXNIP expression and TXR1 association even after treatment with MG132 proteasome inhibitor (Fig. 7A and B), which results in increased inflammasome activation (Fig. 7C, D, F, H and J). Nonetheless LncZFAS1 knockout did not impact pre-cleaved levels of Gsdmd, pro-IL-1β and caspase1 (Fig. 7E, G and I) again indicative of proteasomal regulation of the activated inflammasome.

LncZFAS1 induces TXNIP proteosomal degradation through MIB1 ubiquitination

Proteasomal degradation is mainly regulated by the ubiquitin system[38]. Hence, the levels of TXNIP ubiquitination in oe-LncZFAS1 SH-SY5Y cells were assessed by Co-IP and western blot (Fig. 8A). As expected oe-LncZFAS1 cells showed higher TXNIP association with E3 ubiquitin ligase protein MIB1 following MPP^+ treatment (Fig. 8B). Moreover, LncZFAS1 over-expression significantly induces MIB1 transcriptional and protein levels in SH-SY5Y cells following MPP^+ treatment (Fig. 8C, E and F). To verify that LncZFAS1-induced TXNIP ubiquitination is dependent of MIB1 protein interaction, a MIB1 knockdown SH-SY5Y cell line was generated on the oe-ZFAS1 background (Fig. S3). As hypothesized, MIB1 knockdown rescues TXNIP protein levels in oe-ZFAS1 cells and reduces TXNIP ubiquitination following MPP^+ treatment (Fig. 8D, G and H). In contrast, transfection with lentiviral scramble control had no impact on TXNIP protein levels or ubiquitination (Fig. 8G-H). A series of similar experiments were conducted with sgRNA-ZFAS1 cells, showing decreased TXNIP ubiquitination and MIB1 association (Fig. 8 I and J).

LncZFAS1 interferes with miR590-3p-mediated MIB-1 down-regulation

MicroRNAs (miR) are single small non-coding RNAs that regulate gene expression of a myriad of protein targets[39]. LncZFAS1 significantly downregulates miR590-3p, a putative regulator of MIB1 (Fig. 9A). To assess if miR590-3p regulates MIB1 expression SH-SY5Y cells were treated with a miR590-3p or a miR590-3p inhibitor and respective negative controls, and MIB1 protein levels assessed by western blot. Consistent with *in silico* predictions, miR590-3p treatment prominently decreases MIB1 protein expression. Contrastingly, miR590-3p inhibitor greatly increases MIB1 protein levels (Fig. 9A and B). MiR regulate protein expression post-transcriptionally through direct binding to 3'-untranslation region (3'UTR) inducing translation inhibition or mRNA degradation of their targets. Consistent with this mechanism, SH-SY5Y cells treated with a miR590-3p have significantly lower MIB1 mRNA transcripts, while miR590-3p inhibition significantly increases MIB1 transcriptional expression (Fig. 9C). To validate direct miR590-3p binding to the 3'UTR a MIB1 luciferase reporter system was generated with the WT MIB1 3'UTR (WT-MIB1) or a miR590-3p resistant 3'UTR (mut-MIB1) (Fig. 9D). Consistent with transcriptional data, miR590-3p significantly decreased MIB1-luciferase activity in WT-MIB1 cells but had no impact on mut-MIB1 (Fig. 9E).

LncZFAS1 has been shown to regulate the activity of other miRs[40]. To assess if LncZFAS1 up-regulates MIB1 through interference with miR590-3p, the transcriptional levels of this microRNA were quantified in oe-LcnZFAS1 cells. As expected, oe-LcnZFAS1 SH-SY5Ycells have significantly lower miR590-3p transcripts than the corresponding oe-Vector control cells. In contrast, LcnZFAS1 knockdown significantly increases miR590-3p expression (Fig. 9F). Finally, to confirm that LcnZFAS1 regulates miR590-3p pro-transcriptionally, the intracellular localization of LcnZFAS1 was assessed by FISH staining and confocal microscopy. Consistent with post-transcriptional regulation mechanism, LcnZFAS1 expression mainly localizes in the SH-SY5Y cells cytoplasm following MPP^+ treatment (Fig. 9G). Contrastingly, sgRNA-ZFAS1 cells showed decreased MIB1 transcriptional and protein levels (Fig. 9I-K) and increased miR590-3p expression (Fig. 9L).

Discussion

Exploration of non-coding genome unveiled a panoply of formerly unknown lncRNAs with critical regulatory functions in the pathophysiology of many neurological diseases[41-47]. lncRNAs are mainly expressed during cellular senescence, which represents a major risk factor during neurodegenerative disease development[45, 48]. Moreover, the recent literature exposes an important role of lncRNAs regulating the expression of nearby protein-coding genes and that deregulation of this relationship may lead to brain diseases. The majority of these lncRNAs expressed in the nervous system, have only been identified in genome-wide expression screens; but their involvement in Parkinson's disease (PD) is now a prolific research field[49-52]. Here lncZFAS1 significantly regulated MPP^+-induced pyroptosis and inflammasome activation in human neuroblast cells. To the best of our knowledge this is the first time that a lncRNA shows direct regulation of inflammasome activity in human neuroblast cells, exposing lncZFAS as novel potential therapeutic approach for PD.

Extensive clinical and experimental research suggests that microglial activation and neuroinflammation may be key regulators of dopaminergic neuronal loss in PD[53, 54]. Chronic activation of microglia and an excessive proinflammatory milleu in the brain can result in expression of costimulatory molecules, neuroinflammation and neuronal dysfunction[55-58]. Microglial-mediated neuroinflammation has been reported in many neurodegenerative disorders and uncontrolled NLRP3 inflammasome activation in microglial cells have been observed in the tissue of the substantia nigra in midbrains of PD patients[55]. Both *in vitro* and *in vivo* models of PD have suggested a link between aggregation of α-synuclein, increased mitochondrial ROS and cathepsin B release with the activation of microglial NLRP3 inflammation-mediated pyroptotic cell death of dopaminergic neurons in the substantia nigra[59-61]. In contrast, rare mutations on the NLRP3 inflammasome have been associated with decreased risk PD[62]. Furthermore, several etiological factors associated with neuroinflammation and dopaminergic neuronal loss, such as mitochondrial generation of ROS, mitophagy, loss of function of dopaminergic receptors, and lncRNA are frequently connected with microglial NLRP3 inflammasome activation[61, 62]. Thus, the NLRP3 pathway may provide a new therapeutic avenue for PD treatment. However, the exact mechanism of NLRP3 activation in neural cells remains unclear and a deeper understanding is required to efficiently

target this pathway. Here MPP^+ treatment significantly induced NLRP3 activation and pyroptosis in neuroblast cells (Fig. 1 and 2). Moreover, NLPR3 activation, ASC recruitment, caspase1 cleavage and IL-1β maturation was dependent of TXNIP/TRX1 interaction (Fig. 3-7).

The thioredoxin (Trx) system (composed of NADPH, thioredoxin reductase, and Trx) is a key antioxidant system that protects cells from oxidative stress. Trx1 is a 12-kDa ubiquitous protein with disulfide-reducing activity that is mainly localized in the cytoplasm[63]. TXNIP acts an endogenous Trx inhibitor[64]and together, the Trx-Txnip complex has been recently described as novel protein signaling pathway transducing redox-related signals[63]. TXNIP has a specific arrestin-like domain, which is responsible for highly promiscuous protein–protein interactions. Until now TXNIP has been identified in association with importin-α, transcriptional co-repressors SMRT-mSin3-HDAC (histone deacetylase), Jab1, E3 ubiquitin ligase ITCH, Mybbp1a, and NLRP3, as well as Trx [36, 65-68]. Altogether, these findings expose a central role of TXNIP in a redox signaling complex that results in inflammasome activation. In agreement with this hypothesis, decreased TXNIP expression in neuroblast cells significantly decreased MPP^+ inflammasome activation (Fig. 3-9). A TXNIP centered inflammasome regulation mechanism has not been reported yet. Here we show that increased TXNIP ubiquitination through MIB1 E3 ubiquitin ligase regulates NLRP3 inflammasome activation in neuroblast cells. Mechanistically, MPP^+ activates the NLPR3 inflammasome through miR590-3p up-regulation, which in turn inhibits MIB1-dependent TXNIP ubiquitination. Increase intracellular ROS then activates the TXNIP/TRX redox-sensing complex driving NLRP3/ASC association, caspase 1 activation, cytokine maturation, Grdm cleavage and pyroptosis (Fig. 10). In contrast lncZFAS can inhibit this entire pathway through direct interference with miR590-3p exposing it as an ideal therapeutic target to prevent excessive inflammasome activation and pyroptosis in neuroblast cells and PD. Alternatively, other TXNIP inhibitors might also prove useful for PD treatment. Future studies will assess the impact of TXNIP inhibitors *in vivo* PD models. LncRNA-based therapies are still at their infancy, but recent developments in RNA-delivery technologies opens the doors for the use of lncRNA as novel small-molecule therapeutics to inflammasome-driven neurological diseases such as PD.

References

1. de Rijk MC, Launer LJ, Berger K, Breteler MM, Dartigues JF, Baldereschi M, Fratiglioni L, Lobo A, Martinez-Lage J, Trenkwalder C, Hofman A (2000) Prevalence of Parkinson's disease in Europe: A collaborative study of population-based cohorts. Neurologic Diseases in the Elderly Research Group. Neurology(11 Suppl 5):S21-S23

2. Dorsey ER, Constantinescu R, Thompson JP, Biglan KM, Holloway RG, Kieburtz K, Marshall FJ, Ravina BM, Schifitto G, Siderowf A, Tanner CM (2007) Projected number of people with Parkinson disease in the most populous nations, 2005 through 2030. Neurology(5):384-386. https://10.1212/01.wnl.0000247740.47667.03

3. Zhang XM, Yin M, Zhang MH (2014) Cell-based assays for Parkinson's disease using differentiated human LUHMES cells. Acta Pharmacol Sin(7):945-956. https://10.1038/aps.2014.36

4. Arnot CJ, Gay NJ, Gangloff M (2010) Molecular mechanism that induces activation of Spatzle, the ligand for the Drosophila Toll receptor. J Biol Chem(25):19502-19509. https://10.1074/jbc.M109.098186

5. Schmidt F, Champy P, Seon-Meniel B, Franck X, Raisman-Vozari R, Figadere B (2009) Chemicals possessing a neurotrophin-like activity on dopaminergic neurons in primary culture. Plos One(7):e6215. https://10.1371/journal.pone.0006215

6. Son JH, Chun HS, Joh TH, Cho S, Conti B, Lee JW (1999) Neuroprotection and neuronal differentiation studies using substantia nigra dopaminergic cells derived from transgenic mouse embryos. J Neurosci(1):10-20

7. Langston JW, Langston EB, Irwin I (1984) MPTP-induced parkinsonism in human and non-human primates--clinical and experimental aspects. Acta Neurol Scand Suppl:49-54

8. Gerhard A, Pavese N, Hotton G, Turkheimer F, Es M, Hammers A, Eggert K, Oertel W, Banati RB, Brooks DJ (2006) In vivo imaging of microglial activation with [11C](R)-PK11195 PET in idiopathic Parkinson's disease. Neurobiol Dis(2):404-412. https://10.1016/j.nbd.2005.08.002

9. He Y, Appel S, Le W (2001) Minocycline inhibits microglial activation and protects nigral cells after 6-hydroxydopamine injection into mouse striatum. Brain Res(1-2):187-193. https://10.1016/s0006-8993(01)02681-6

10. Wu DC, Jackson-Lewis V, Vila M, Tieu K, Teismann P, Vadseth C, Choi DK, Ischiropoulos H, Przedborski S (2002) Blockade of microglial activation is neuroprotective in the 1-methyl-4-phenyl-1,2,3,6-tetrahydropyridine mouse model of Parkinson disease. J Neurosci(5):1763-1771

11. Edison P, Ahmed I, Fan Z, Hinz R, Gelosa G, Ray CK, Walker Z, Turkheimer FE, Brooks DJ (2013) Microglia, amyloid, and glucose metabolism in Parkinson's disease with and without dementia. Neuropsychopharmacol(6):938-949. https://10.1038/npp.2012.255

12. Schroder K, Tschopp J (2010) The inflammasomes. Cell(6):821-832. https://10.1016/j.cell.2010.01.040

13. Rathinam VA, Fitzgerald KA (2016) Inflammasome complexes: Emerging mechanisms and effector functions. Cell(4):792-800. https://10.1016/j.cell.2016.03.046

14. Jo EK, Kim JK, Shin DM, Sasakawa C (2016) Molecular mechanisms regulating NLRP3 inflammasome activation. Cell Mol Immunol(2):148-159. https://10.1038/cmi.2015.95

15. Guo H, Callaway JB, Ting JP (2015) Inflammasomes: Mechanism of action, role in disease, and therapeutics. Nat Med(7):677-687. https://10.1038/nm.3893

16. Ozaki E, Campbell M, Doyle SL (2015) Targeting the NLRP3 inflammasome in chronic inflammatory diseases: Current perspectives. J Inflamm Res:15-27. https://10.2147/JIR.S51250

17. Lee E, Hwang I, Park S, Hong S, Hwang B, Cho Y, Son J, Yu JW (2019) MPTP-driven NLRP3 inflammasome activation in microglia plays a central role in dopaminergic neurodegeneration. Cell Death Differ(2):213-228. https://10.1038/s41418-018-0124-5

18. Shao BZ, Xu ZQ, Han BZ, Su DF, Liu C (2015) NLRP3 inflammasome and its inhibitors: A review. Front Pharmacol:262. https://10.3389/fphar.2015.00262

19. Broz P, Dixit VM (2016) Inflammasomes: Mechanism of assembly, regulation and signalling. Nat Rev Immunol(7):407-420. https://10.1038/nri.2016.58

20. Gurung P, Lukens JR, Kanneganti TD (2015) Mitochondria: Diversity in the regulation of the NLRP3 inflammasome. Trends Mol Med(3):193-201. https://10.1016/j.molmed.2014.11.008

21. Heid ME, Keyel PA, Kamga C, Shiva S, Watkins SC, Salter RD (2013) Mitochondrial reactive oxygen species induces NLRP3-dependent lysosomal damage and inflammasome activation. J Immunol(10):5230-5238. https://10.4049/jimmunol.1301490

22. Sorbara MT, Girardin SE (2011) Mitochondrial ROS fuel the inflammasome. Cell Res(4):558-560. https://10.1038/cr.2011.20

23. Vanaja SK, Rathinam VA, Fitzgerald KA (2015) Mechanisms of inflammasome activation: Recent advances and novel insights. Trends Cell Biol(5):308-315. https://10.1016/j.tcb.2014.12.009

24. Yao RW, Wang Y, Chen LL (2019) Cellular functions of long noncoding RNAs. Nat Cell Biol(5):542-551. https://10.1038/s41556-019-0311-8

25. Poliseno L, Salmena L, Zhang J, Carver B, Haveman WJ, Pandolfi PP (2010) A coding-independent function of gene and pseudogene mRNAs regulates tumour biology. Nature(7301):1033-1038. https://10.1038/nature09144

26. Salmena L, Poliseno L, Tay Y, Kats L, Pandolfi PP (2011) A ceRNA hypothesis: The Rosetta Stone of a hidden RNA language? Cell(3):353-358. https://10.1016/j.cell.2011.07.014

27. Elkouris M, Kouroupi G, Vourvoukelis A, Papagiannakis N, Kaltezioti V, Matsas R, Stefanis L, Xilouri M, Politis PK (2019) Long non-coding RNAs associated with Neurodegeneration-Linked genes are reduced in parkinson's disease patients. Front Cell Neurosci:58. https://10.3389/fncel.2019.00058

28. Hadjicharalambous MR, Roux BT, Feghali-Bostwick CA, Murray LA, Clarke DL, Lindsay MA (2018) Long non-coding RNAs are central regulators of the IL-1beta-Induced inflammatory response in normal and idiopathic pulmonary lung fibroblasts. Front Immunol:2906. https://10.3389/fimmu.2018.02906

29. Askarian-Amiri ME, Crawford J, French JD, Smart CE, Smith MA, Clark MB, Ru K, Mercer TR, Thompson ER, Lakhani SR, Vargas AC, Campbell IG, Brown MA, Dinger ME, Mattick JS (2011) SNORD-host RNA Zfas1 is a regulator of mammary development and a potential marker for breast cancer. Rna(5):878-891. https://10.1261/rna.2528811

30. Zhang Y, Sun L, Xuan L, Pan Z, Li K, Liu S, Huang Y, Zhao X, Huang L, Wang Z, Hou Y, Li J, Tian Y, Yu J, Han H, Liu Y, Gao F, Zhang Y, Wang S, Du Z, Lu Y, Yang B (2016) Reciprocal changes of circulating long Non-Coding RNAs ZFAS1 and CDR1AS predict acute myocardial infarction. Sci Rep:22384. https://10.1038/srep22384

31. Wu T, Wu D, Wu Q, Zou B, Huang X, Cheng X, Wu Y, Hong K, Li P, Yang R, Li Y, Cheng Y (2017) Knockdown of long Non-Coding RNA-ZFAS1 protects cardiomyocytes against acute myocardial infarction via Anti-Apoptosis by regulating miR-150/CRP. J Cell Biochem(10):3281-3289. https://10.1002/jcb.25979

32. Ye Y, Gao X, Yang N (2018) LncRNA ZFAS1 promotes cell migration and invasion of fibroblast-like synoviocytes by suppression of miR-27a in rheumatoid arthritis. Hum Cell(1):14-21. https://10.1007/s13577-017-0179-5

33. Dong D, Mu Z, Wang W, Xin N, Song X, Shao Y, Zhao C (2017) Prognostic value of long noncoding RNA ZFAS1 in various carcinomas: A meta-analysis. Oncotarget(48):84497-84505. https://10.18632/oncotarget.21100

34. Makkar R, Behl T, Bungau S, Kumar A, Arora S (2020) Understanding the role of inflammasomes in rheumatoid arthritis. Inflammation(6):2033-2047. https://10.1007/s10753-020-01301-1

35. He A, He S, Li X, Zhou L (2019) ZFAS1: A novel vital oncogenic lncRNA in multiple human cancers. Cell Prolif(1):e12513. https://10.1111/cpr.12513

36. Zhou R, Tardivel A, Thorens B, Choi I, Tschopp J (2010) Thioredoxin-interacting protein links oxidative stress to inflammasome activation. Nat Immunol(2):136-140. https://10.1038/ni.1831

37. Filhoulaud G, Benhamed F, Pagesy P, Bonner C, Fardini Y, Ilias A, Movassat J, Burnol AF, Guilmeau S, Kerr-Conte J, Pattou F, Issad T, Postic C (2019) O-GlcNacylation links TxNIP to inflammasome activation in pancreatic beta cells. Front Endocrinol (Lausanne):291. https://10.3389/fendo.2019.00291

38. Lopez-Castejon G (2020) Control of the inflammasome by the ubiquitin system. Febs J(1):11-26. https://10.1111/febs.15118

39. Wang H, Cai J (2017) The role of microRNAs in heart failure. Biochim Biophys Acta Mol Basis Dis(8):2019-2030. https://10.1016/j.bbadis.2016.11.034

40. Dong D, Mu Z, Zhao C, Sun M (2018) ZFAS1: A novel tumor-related long non-coding RNA. Cancer Cell Int:125. https://10.1186/s12935-018-0623-y

41. Akula N, Barb J, Jiang X, Wendland JR, Choi KH, Sen SK, Hou L, Chen DT, Laje G, Johnson K, Lipska BK, Kleinman JE, Corrada-Bravo H, Detera-Wadleigh S, Munson PJ, Mcmahon FJ (2014) RNA-sequencing of the brain transcriptome implicates dysregulation of neuroplasticity, circadian rhythms and GTPase binding in bipolar disorder. Mol Psychiatry(11):1179-1185. https://10.1038/mp.2013.170

42. Barry G (2014) Integrating the roles of long and small non-coding RNA in brain function and disease. Mol Psychiatry(4):410-416. https://10.1038/mp.2013.196

43. Johnson R, Richter N, Jauch R, Gaughwin PM, Zuccato C, Cattaneo E, Stanton LW (2010) Human accelerated region 1 noncoding RNA is repressed by REST in Huntington's disease. Physiol Genomics(3):269-274. https://10.1152/physiolgenomics.00019.2010

44. Ng SY, Lin L, Soh BS, Stanton LW (2013) Long noncoding RNAs in development and disease of the central nervous system. Trends Genet(8):461-468. https://10.1016/j.tig.2013.03.002

45. Sarkar SN, Russell AE, Engler-Chiurazzi EB, Porter KN, Simpkins JW (2019) MicroRNAs and the genetic nexus of brain aging, neuroinflammation, neurodegeneration, and brain trauma. Aging Dis(2):329-352. https://10.14336/AD.2018.0409

46. Wang S, Zhang X, Guo Y, Rong H, Liu T (2017) The long noncoding RNA HOTAIR promotes Parkinson's disease by upregulating LRRK2 expression. Oncotarget(15):24449-24456. https://10.18632/oncotarget.15511

47. Faghihi MA, Modarresi F, Khalil AM, Wood DE, Sahagan BG, Morgan TE, Finch CE, St LGR, Kenny PJ, Wahlestedt C (2008) Expression of a noncoding RNA is elevated in Alzheimer's disease and drives rapid feed-forward regulation of beta-secretase. Nat Med(7):723-730. https://10.1038/nm1784

48. Chakrabarti S, Mohanakumar KP (2016) Aging and neurodegeneration: A tangle of models and mechanisms. Aging Dis(2):111-113. https://10.14336/AD.2016.0312

49. Marki S, Goblos A, Szlavicz E, Torok N, Balicza P, Bereznai B, Takats A, Engelhardt J, Klivenyi P, Vecsei L, Molnar MJ, Nagy N, Szell M (2018) The rs13388259 intergenic polymorphism in the genomic context of the BCYRN1 gene is associated with parkinson's disease in the hungarian population. Parkinsons Dis:9351598. https://10.1155/2018/9351598

50. Ni Y, Huang H, Chen Y, Cao M, Zhou H, Zhang Y (2017) Investigation of long non-coding RNA expression profiles in the substantia nigra of parkinson's disease. Cell Mol Neurobiol(2):329-338. https://10.1007/s10571-016-0373-0

51. Saracchi E, Fermi S, Brighina L (2014) Emerging candidate biomarkers for Parkinson's disease: A review. Aging Dis(1):27-34. https://10.14366/AD.2014.050027

52. Soreq L, Guffanti A, Salomonis N, Simchovitz A, Israel Z, Bergman H, Soreq H (2014) Long non-coding RNA and alternative splicing modulations in Parkinson's leukocytes identified by RNA sequencing. Plos Comput Biol(3):e1003517. https://10.1371/journal.pcbi.1003517

53. Jellinger KA (2012) Neuropathology of sporadic Parkinson's disease: Evaluation and changes of concepts. Mov Disord(1):8-30. https://10.1002/mds.23795

54. Rocha NP, de Miranda AS, Teixeira AL (2015) Insights into neuroinflammation in parkinson's disease: From biomarkers to Anti-Inflammatory based therapies. Biomed Res Int:628192. https://10.1155/2015/628192

55. Gordon R, Albornoz EA, Christie DC, Langley MR, Kumar V, Mantovani S, Robertson A, Butler MS, Rowe DB, O'Neill LA, Kanthasamy AG, Schroder K, Cooper MA, Woodruff TM (2018) Inflammasome inhibition prevents alpha-synuclein pathology and dopaminergic neurodegeneration in mice. Sci Transl Med(465). https://10.1126/scitranslmed.aah4066

56. Kinney JW, Bemiller SM, Murtishaw AS, Leisgang AM, Salazar AM, Lamb BT (2018) Inflammation as a central mechanism in Alzheimer's disease. Alzheimers Dement (N Y):575-590. https://10.1016/j.trci.2018.06.014

57. Moss DW, Bates TE (2001) Activation of murine microglial cell lines by lipopolysaccharide and interferon-gamma causes NO-mediated decreases in mitochondrial and cellular function. Eur J Neurosci(3):529-538. https://10.1046/j.1460-9568.2001.01418.x

58. Nayak D, Roth TL, Mcgavern DB (2014) Microglia development and function. Annu Rev Immunol:367-402. https://10.1146/annurev-immunol-032713-120240

59. Beraud D, Twomey M, Bloom B, Mittereder A, Ton V, Neitzke K, Chasovskikh S, Mhyre TR, Maguire-Zeiss KA (2011) Alpha-Synuclein alters Toll-Like receptor expression. Front Neurosci:80. https://10.3389/fnins.2011.00080

60. Codolo G, Plotegher N, Pozzobon T, Brucale M, Tessari I, Bubacco L, de Bernard M (2013) Triggering of inflammasome by aggregated alpha-synuclein, an inflammatory response in synucleinopathies. Plos One(1):e55375. https://10.1371/journal.pone.0055375

61. Sarkar S, Malovic E, Harishchandra DS, Ghaisas S, Panicker N, Charli A, Palanisamy BN, Rokad D, Jin H, Anantharam V, Kanthasamy A, Kanthasamy AG (2017) Mitochondrial impairment in microglia amplifies NLRP3 inflammasome proinflammatory signaling in cell culture and animal models of Parkinson's disease. NPJ Parkinsons Dis:30. https://10.1038/s41531-017-0032-2

62. von Herrmann KM, Salas LA, Martinez EM, Young AL, Howard JM, Feldman MS, Christensen BC, Wilkins OM, Lee SL, Hickey WF, Havrda MC (2018) NLRP3 expression in mesencephalic neurons and

characterization of a rare NLRP3 polymorphism associated with decreased risk of Parkinson's disease. NPJ Parkinsons Dis:24. https://10.1038/s41531-018-0061-5

63. Yoshihara E, Masaki S, Matsuo Y, Chen Z, Tian H, Yodoi J (2014) Thioredoxin/Txnip: Redoxisome, as a redox switch for the pathogenesis of diseases. Front Immunol:514. https://10.3389/fimmu.2013.00514

64. Nishiyama A, Matsui M, Iwata S, Hirota K, Masutani H, Nakamura H, Takagi Y, Sono H, Gon Y, Yodoi J (1999) Identification of thioredoxin-binding protein-2/vitamin D(3) up-regulated protein 1 as a negative regulator of thioredoxin function and expression. J Biol Chem(31):21645-21650. https://10.1074/jbc.274.31.21645

65. Ago T, Liu T, Zhai P, Chen W, Li H, Molkentin JD, Vatner SF, Sadoshima J (2008) A redox-dependent pathway for regulating class II HDACs and cardiac hypertrophy. Cell(6):978-993. https://10.1016/j.cell.2008.04.041

66. Jeon JH, Lee KN, Hwang CY, Kwon KS, You KH, Choi I (2005) Tumor suppressor VDUP1 increases p27(kip1) stability by inhibiting JAB1. Cancer Res(11):4485-4489. https://10.1158/0008-5472.CAN-04-2271

67. Yamaguchi F, Takata M, Kamitori K, Nonaka M, Dong Y, Sui L, Tokuda M (2008) Rare sugar D-allose induces specific up-regulation of TXNIP and subsequent G1 cell cycle arrest in hepatocellular carcinoma cells by stabilization of p27kip1. Int J Oncol(2):377-385

68. Yoshihara E, Fujimoto S, Inagaki N, Okawa K, Masaki S, Yodoi J, Masutani H (2010) Disruption of TBP-2 ameliorates insulin sensitivity and secretion without affecting obesity. Nat Commun:127. https://10.1038/ncomms1127

Tables

Table 1 Antibodies and dilution

Antibodies	Dilution (application)	Source and Cat#
NLRP3	1:1000 (WB)	Abcam-ab214185
Gsdmd	1:1000 (WB)	Abcam-ab210070
ASC	1:100 (IP)	Abcam-ab151700
TXNIP	1:1000 (WB), 1:200 (IP)	Abcam-ab188865
TRX1	1:100 (IP)	Abcam-ab26320
MIB1	1:1000 (WB)	Abcam-ab124929
IL1β	1:1000 (WB)	Abcam-ab229696
Ubiquitin	1:2000 (WB)	Abcam-ab7780
Caspase-1	1:1000 (WB)	CST-89332
GAPDH	1:10000 (WB)	Abcam-ab181602

Table 2 qRT-PCR protocol

Step1：95℃	15min
Step2: 95℃	5s
55℃	5s
70℃	30s
Step2：30~40 cycles	
Step3：4℃	Dissociation analysis

Table 3 Primers used in Quantitative Real-Time PCR

Gene Target	Primers	Sequence 5’-3’
LncRNAZFAS1	Forward	5’- AACCAGGCTTTGATTGAACC -3’
	Reverse	5’-ATTCCATCGCCAGTTTCT -3’
TXNIP	Forward	5’-CAACTTGCTGCCCGACAAAA-3’
	Reverse	5’-TGGGTGGCATGCAAGGTATT-3’
MIB1	Forward	5’-TGGGGATTCATTGCTGCTAGAT-3’
	Reverse	5’-ACAGTGTAAGAGGGCTAGAGAC -3
GAPDH	Forward	5’-GGTCTCCTCTGACTTCAACA -3’
	Reverse	5’- GTGAGGGTCTCTCTCTTCCT -3’
Has-miR-590-3p	Forward	5’- AAAGATTCCAAGAAGCTAAGGGTG -3’
	Reverse	5’- CCTAACTGGTTTCCTGTGCCTA -3’
U6	Forward	5’- CTCGCTTCGGCAGCACA -3’
	Reverse	5’- AACGCTTCACGAATTTGCGT -3’

Figures

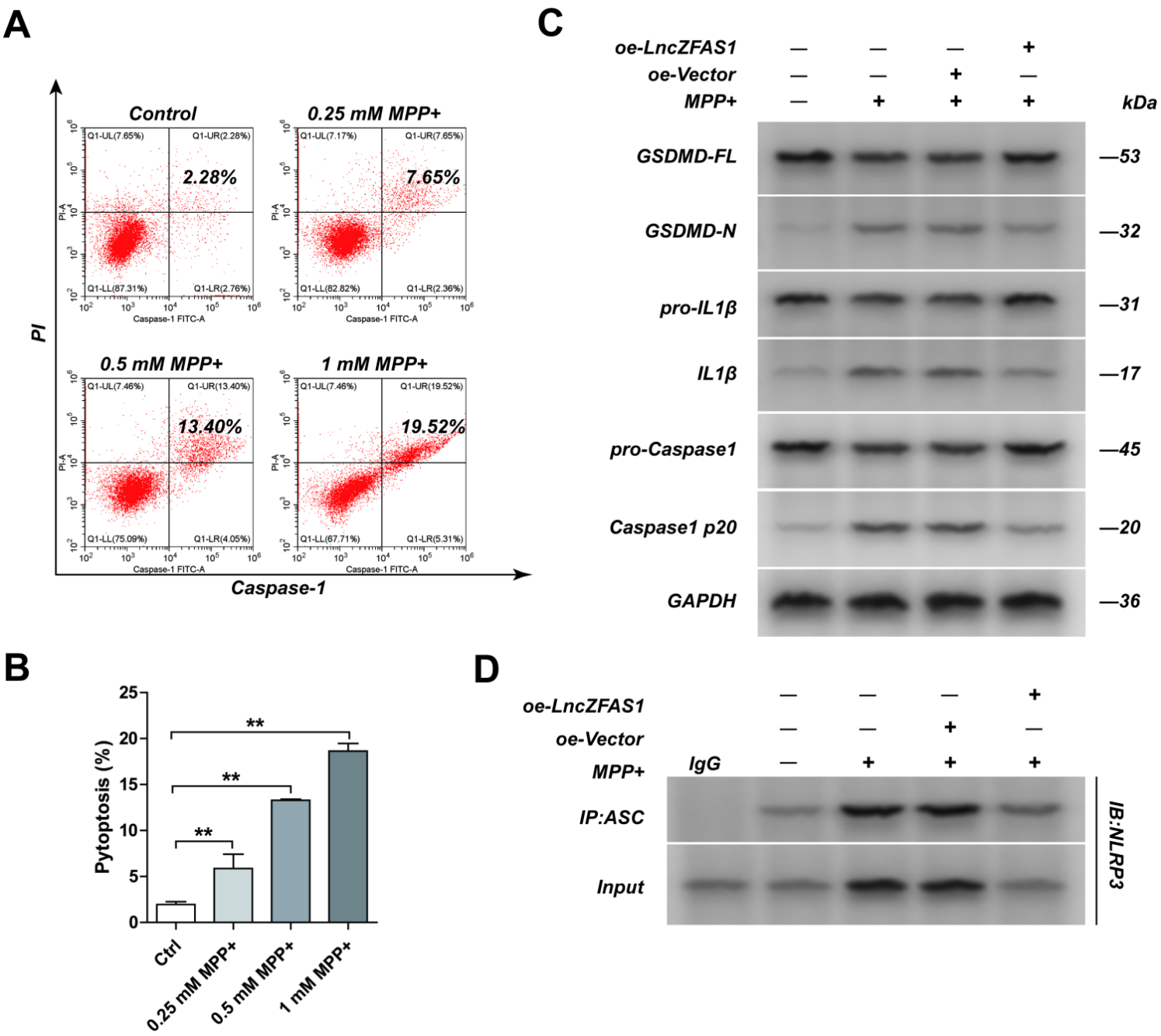

Figure 1

Fig. 1 MPP+ induces SH-SY5Y cells pyroptosis through inflammasome activation. A) SH-SY5Y cells were treated with MPP+ (0.25, 0.5,1 mM) for 24 h and frequency of pyroptotic cells measure by flow cytometry as Propidium idodide and caspase-1 active double positive cells. B) Summary data for the frequency pf pyroptotic SH-SY5Y cells in the indicated group, measured as in A. C) Expression of inflammasome effector proteins Gsdmd-full length, Gsdmd-N, pro-IL1β, IL-1β, pro-caspase1, caspase1 p20 in SH-SY5Y cells from the indicated group, detected by western blot assay. D) NLRP3/ASC interaction detected following immunoprecipitation with anti- ASC or control IgG antibody. Results represent mean ± SD of three individual experiments for each condition, performed in triplicate. *p<0.05, **p<0.01.

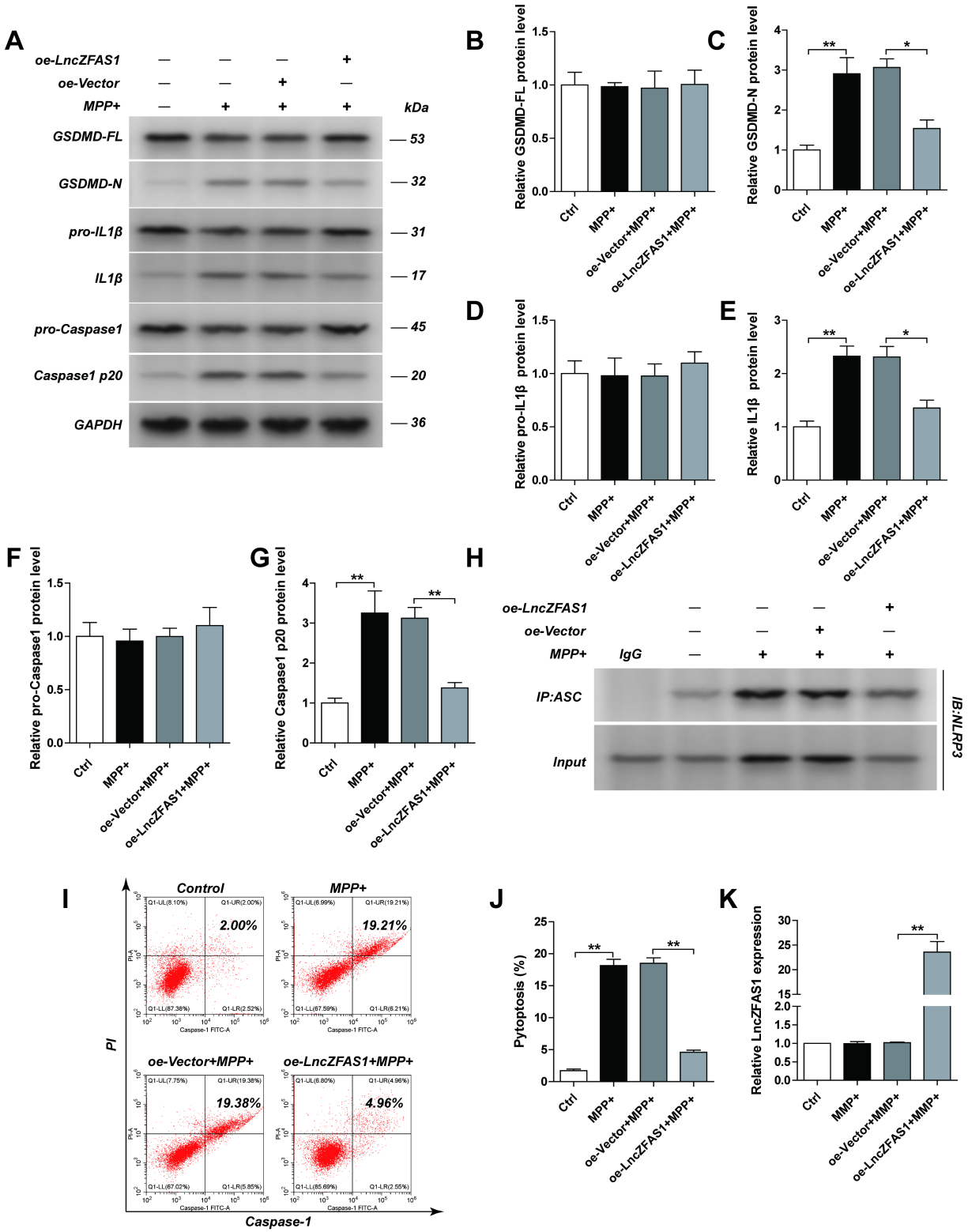

Figure 2

Fig. 2 LncZFAS1 over-expression inhibits inflammasome activation and pyroptosis in SH-SY5Y cells. SH-SY5Y cells were stably transfected with lentiviral vector for LncZFAS over expression or corresponding empty vector control. SH-SY5Y transfected cells were treated with MPP+ (1 mM) for 24h and the expression of Gsdmd-full length, Gsdmd-N, pro-IL1β, IL-1β, pro-caspase1,caspase1 p20 in SH-SY5Y cells detected by western blot assay (A). B-H) Relative expression of Gsdmd-full length (B), Gsdmd-N (C), pro-

IL1β (D), IL-1β (E), pro-caspase1 (F), caspase1 p20 (H) measured by Western blot densitometry as in A. H) NLRP3/ASC interaction detected by immunoprecipitation with anti- ASC or control IgG antibody (G). Frequency of pyroptotic SH-SY5Y transfected cells following MPP+ treatment, measured by flow cytometry (I-J). The expression of LncZFAS1 in the indicated group was measured by qPCR (K). Data represented as mean ± SD of three individual experiments for each condition, performed in triplicate. *p < 0.05, **p < 0.01.

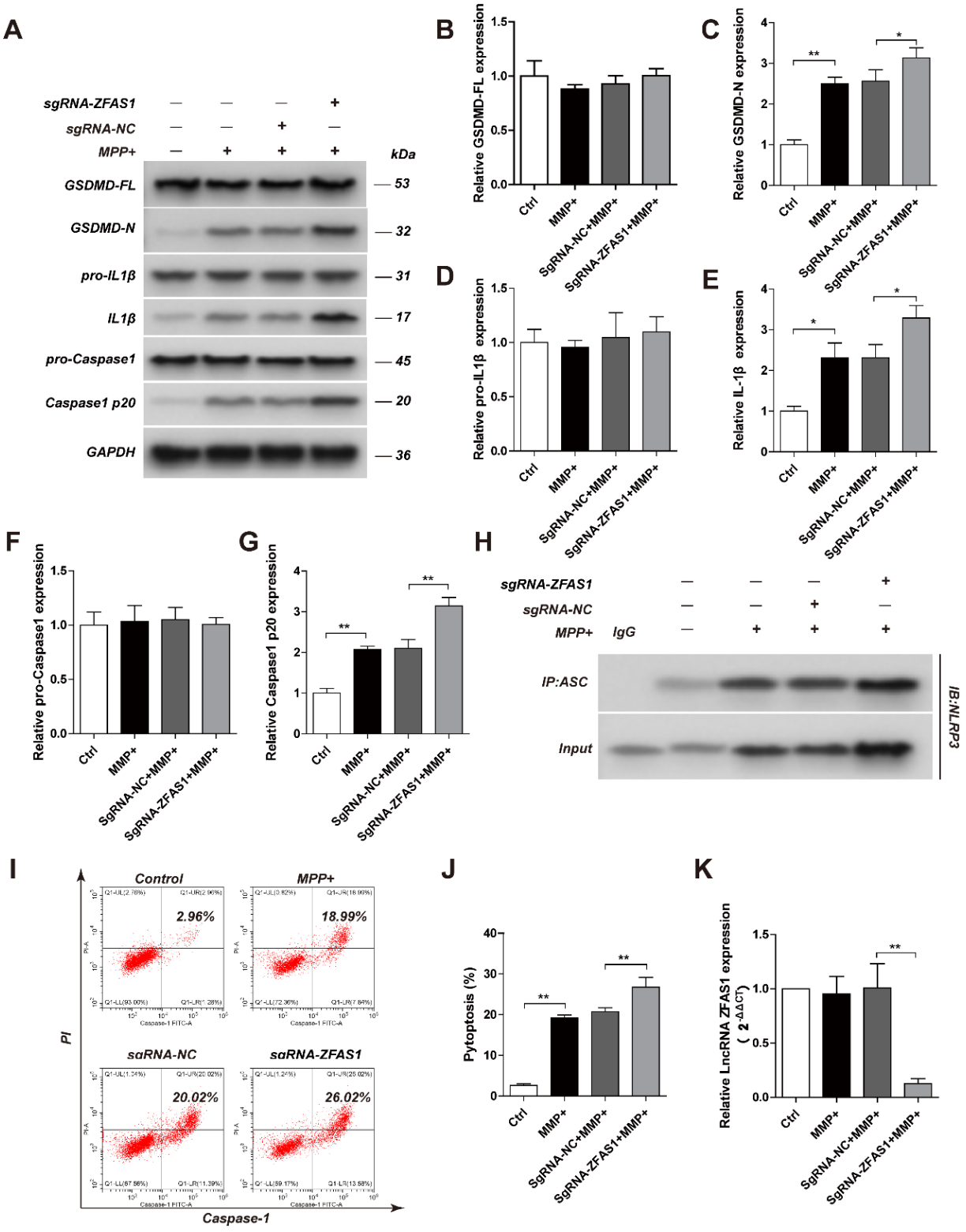

Figure 3

Fig. 3 LncZFAS1 Knockout induces inflammasome activation and pyroptosis in SH-SY5Y cells. LncZFAS1 was stably knockout by Crispr-cas9 plasmid in SH-SY5Y cells (sgRNA-ZFAS1) or corresponding negative control (sgRNA-NC), which were then treated with MPP+ (1 mM) for 24h. Expression of Gsdmd-full length (A, B), Gsdmd-N (A, C), pro-IL1β (A, D), IL-1β (A, E), pro-caspase1(A, F), caspase1 p20 (A, G) of SH-SY5Y transfected cells were detected by western blot assay, and cell lysates were immunoprecipitated with anti-ASC antibody or control IgG followed by Co-IP assay to determine the interaction of Nlrp3 and ASC (G). The pyroptosis ratio of SH-SY5Y cells in the indicated group was measured by flow cytometric analysis (I-J). LncZFAS1 knockout was validated by qPCR (K). Data represented as mean ± SD of three individual experiments for each condition, performed in triplicate. *p < 0.05, **p < 0.01.

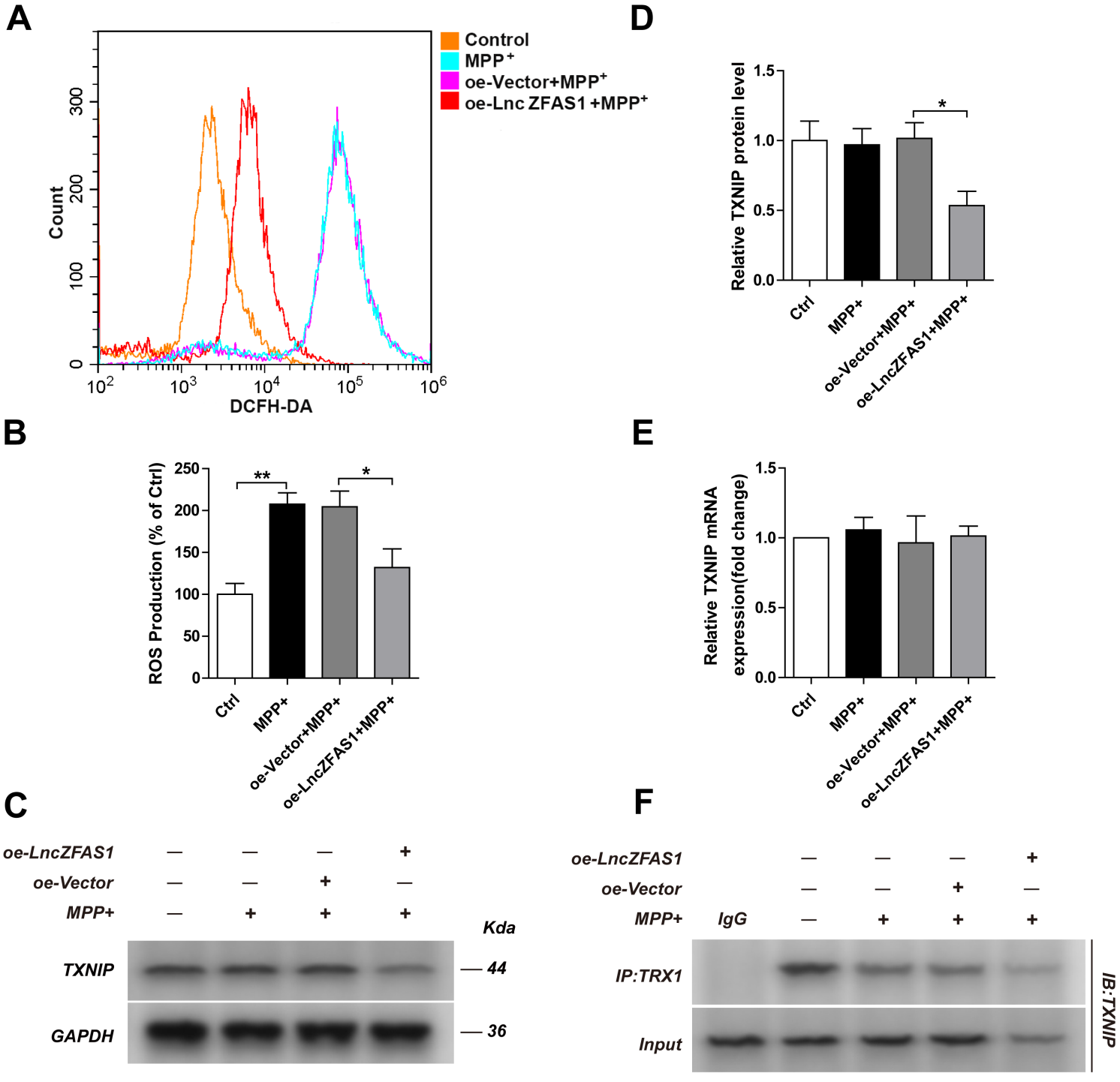

Figure 4

Fig. 4 LncZFAS1 over-expression blocks MPP+ induced oxidative stress through TRX1/TXNIP redox signaling complex. SH-SY5Y cells were stably transfected with lentiviral vector for LncZFAS over expression or corresponding empty vector control. SH-SY5Y transfected cells were treated with MPP+ (1 mM) for 24h and intracellular ROS measured by flow cytometry (A and B). Protein and transcriptional expression of TXNIP was detected by western blot assay (C, D) or qRT-PCR (E). TXNIP/TRX1 interaction was detected by immunoprecipitation with anti-TRX1 antibody or control IgG (F). Data represented as mean ± SD of three individual experiments for each condition, performed in triplicate. *$p < 0.05$, **$p < 0.01$.

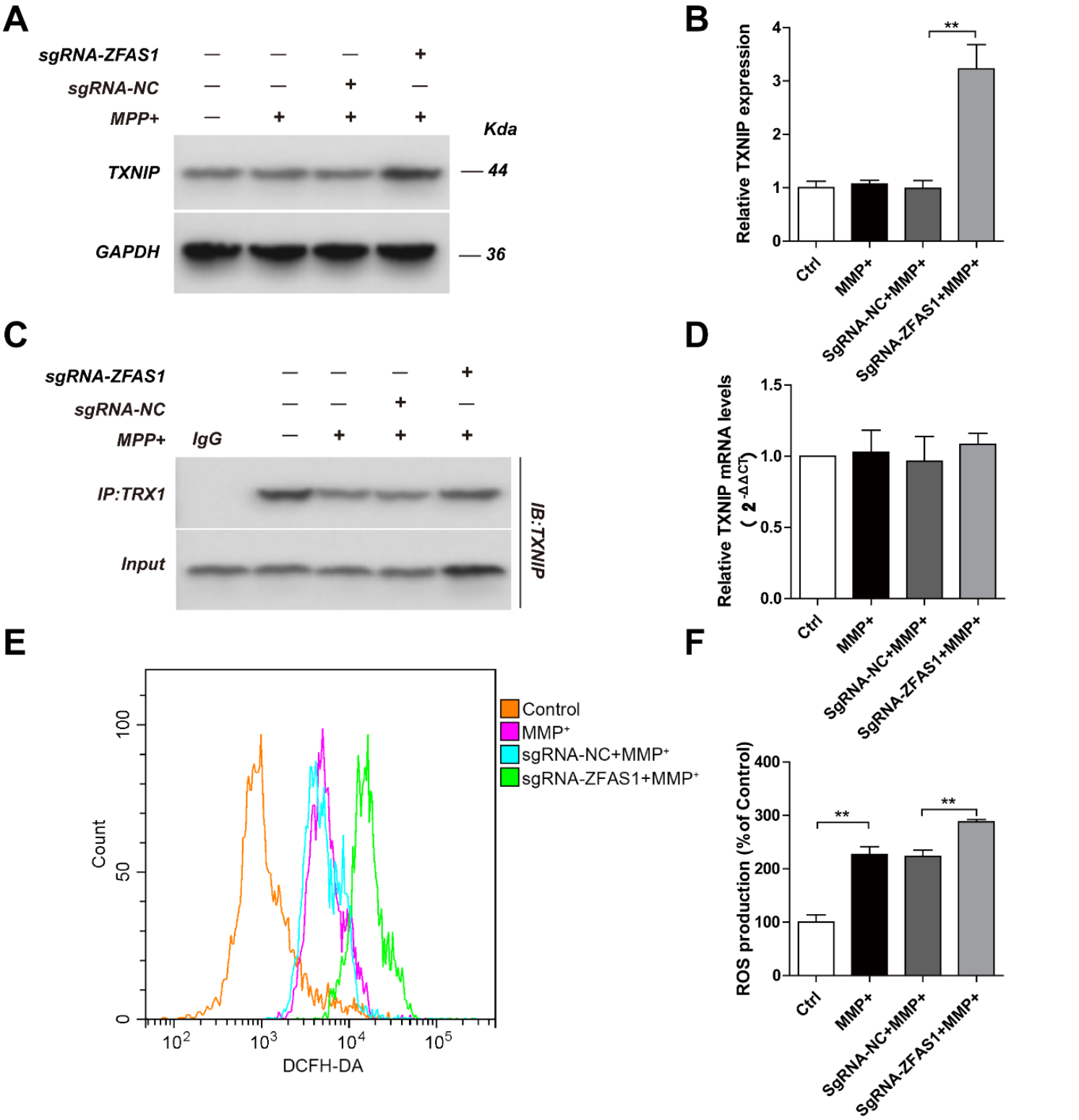

Figure 5

Fig. 5 LncZFAS1 knockout enhances MPP+ induced oxidative stress through TRX1/TXNIP redox signaling complex. LncZFAS1 was stably knockout by Crispr-cas9 plasmid in SH-SY5Y cells (sgRNA-ZFAS1) or corresponding negative control (sgRNA-NC), which were then treated with MPP+ (1 mM) for 24h. The expression of TXNIP (A, B) was detected by western blot assay, and the cell lysates were immunoprecipitated with anti- TRX1 antibody or control IgG followed by Co-IP assay to determine the

interaction of TXNIP and TRX1 (C). TXNIP mRNA levels of the indicated groups were measured by qPCR(D). ROS production of sgRNA-ZFAS1 SH-SY5Y cells treated as in A were measured by flow cytometric analysis (E-F). Data represented as mean ± SD of three individual experiments for each condition, performed in triplicate. *p < 0.05, **p < 0.01.

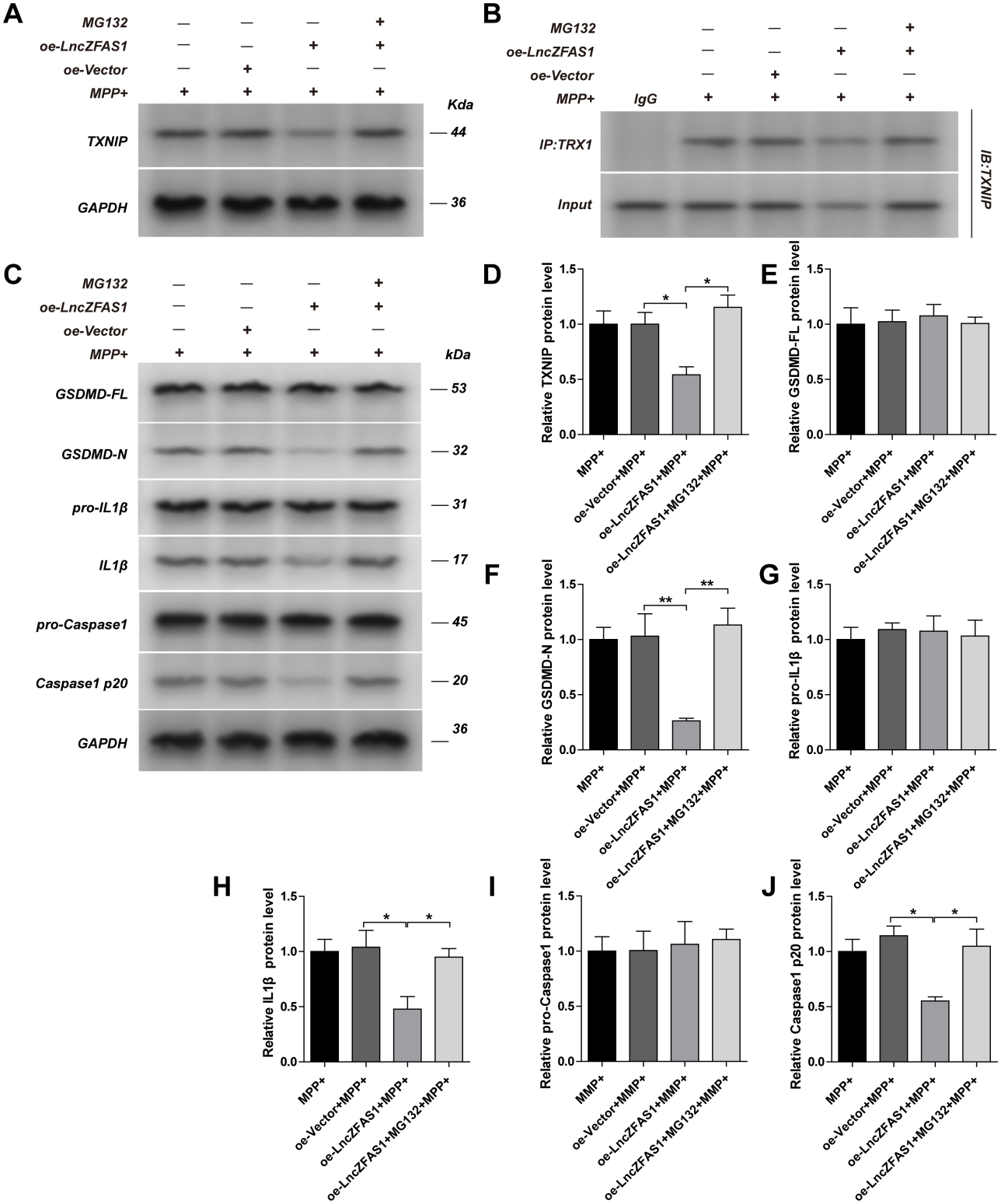

Figure 6

Fig. 6 LncZFAS1 overexpression inhibits inflammasome activation through TXNIP proteasomal degradation. SH-SY5Y cells were stably transfected with lentiviral vector for LncZFAS over expression or corresponding empty vector control. SH-SY5Y transfected cells were treated with MPP+ (1 mM) or co-treated with MG132 (1 μM) for 24h and the expression of TXNIP (A, D), Gsdmd-full length (C, E), Gsdmd-N (C, F), pro-IL1β (C, G), IL-1β (C, H), pro-caspase1(C, I), caspase1 p20 (C, J) were detected by western blot assay. TXNIP/TRX1 interaction was detected by immunoprecipitation with anti-TRX1 or control IgG antibody (B). Data represented as mean ± SD of three individual experiments for each condition, performed in triplicate. *$p < 0.05$, **$p < 0.01$.

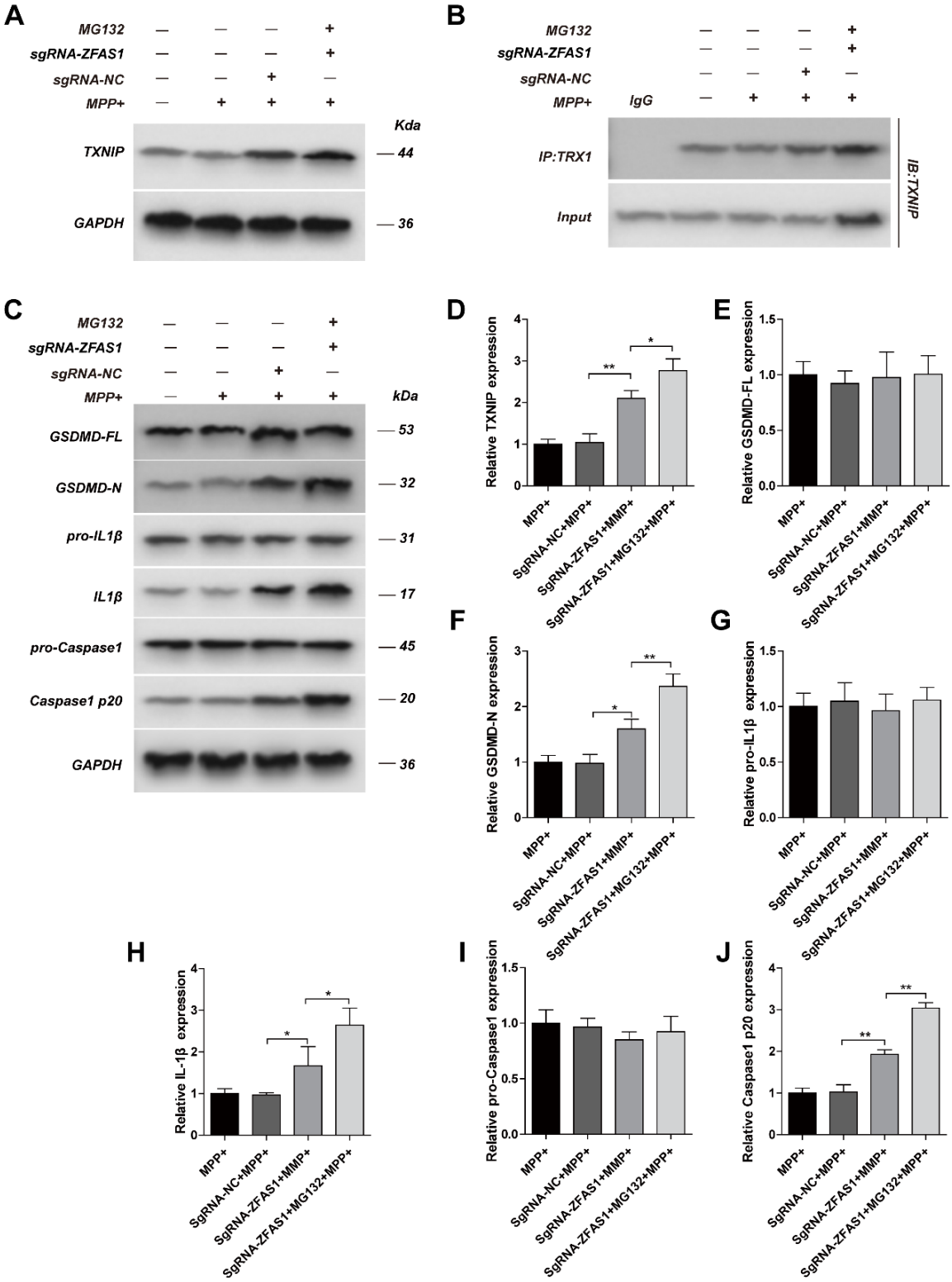

Figure 7

Fig. 7 LncZFAS1 knockout increases TXNIP expression in MPP+-treated SH-SY5Y cells. LncZFAS1 was stably knockout by Crispr-cas9 plasmid in SH-SY5Y cells (sgRNA-ZFAS1) or corresponding negative control (sgRNA-NC), which were then treated with MPP+ (1 mM) or co-treated with MG132 (1 μM) for 24 h. The expression of TXNIP (A, D), Gsdmd-full length (C, E), Gsdmd-N (C, F),pro-IL1β (C, G),IL-1β (C, H),pro-caspase1 (C, I),caspase1 p20 (C, J) of transfected cells were detected by western blot assay. TXNIP/TRX1

interaction was detected by immunoprecipitation with anti-TRX1 or control IgG antibody (B). Data represented as mean ± SD of three individual experiments for each condition, performed in triplicate. *p < 0.05, **p < 0.01.

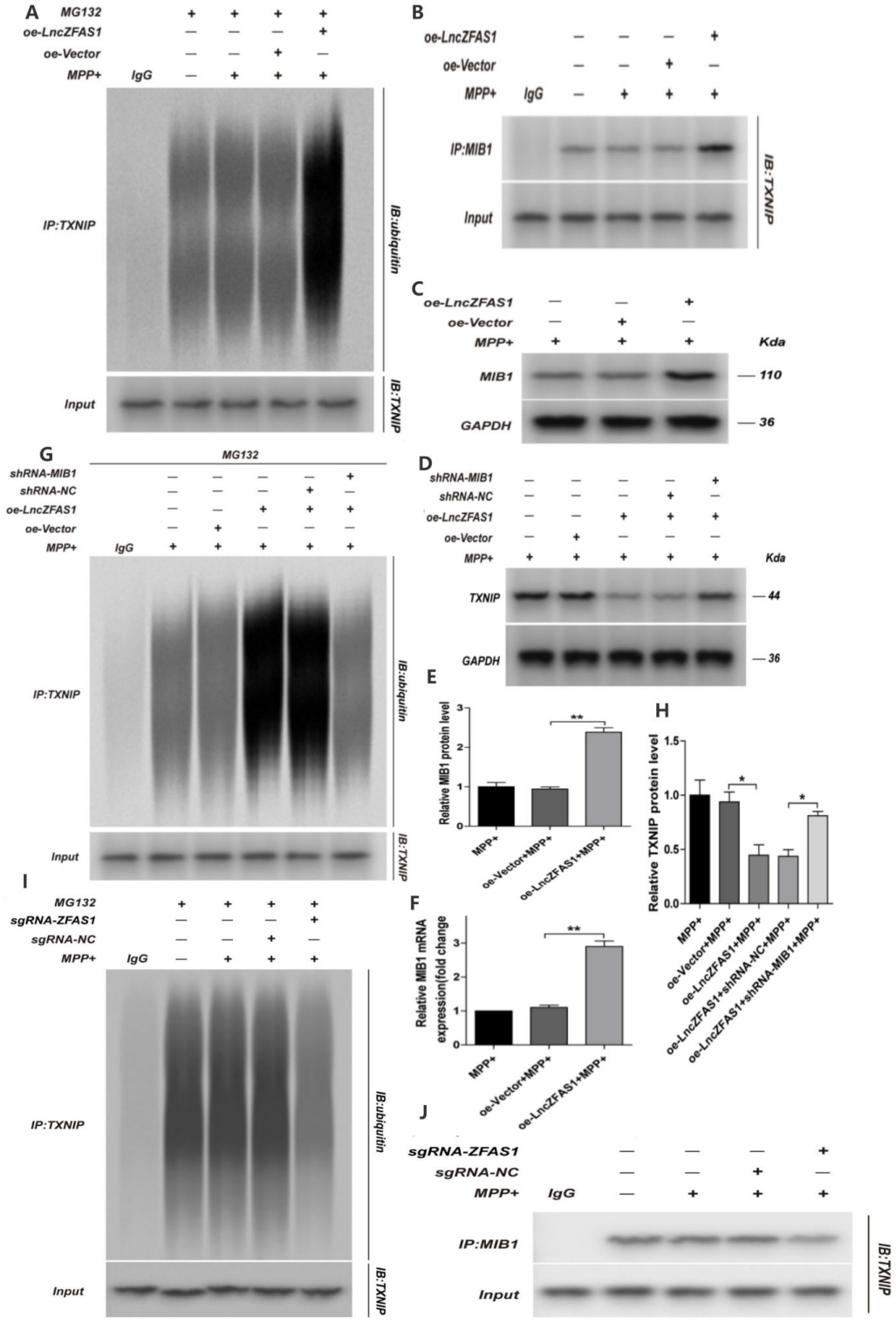

Figure 8

Fig. 8 LncZFAS1 regulates TXNIP ubiquitination. SH-SY5Y cells were stably transfected with lentiviral vector for LncZFAS over expression or corresponding empty vector control. Transfected cells were then

treated with MPP+ (1 mM) or co-treated with MG132 (1 μM) for 24h, and specific ubiquitination was assessed by immunoprecipitation with anti-TXNIP antibody, followed by immunoblot with anti-ubiquitin antibody (A). TXNIP/MIB1 interaction was determined by immunoprecipitation with anti-MIB1 or control IgG antibody (B). MIB1 expression was quantified by western blot (C, E) and qRT-PCR (F). A, B, C, G and H results are representative of three independent experiments. LncZFAS1 stably knockout SH-SY5Y cells (sgRNA-ZFAS1) were treated with MPP+ (1 mM) or co-treated with MG132 (1 μM) for 24h and cell extracts immunoprecipitated with anti-TXNIP antibody, followed by immunoblot with anti-ubiquitin antibody (I). TXNIP/MIB1 interaction was detected by immunoprecipitation with anti- MIB1 antibody or control IgG (J). Data represented as mean ± SD of three individual experiments for each condition, performed in triplicate. *$p < 0.05$, **$p < 0.01$.

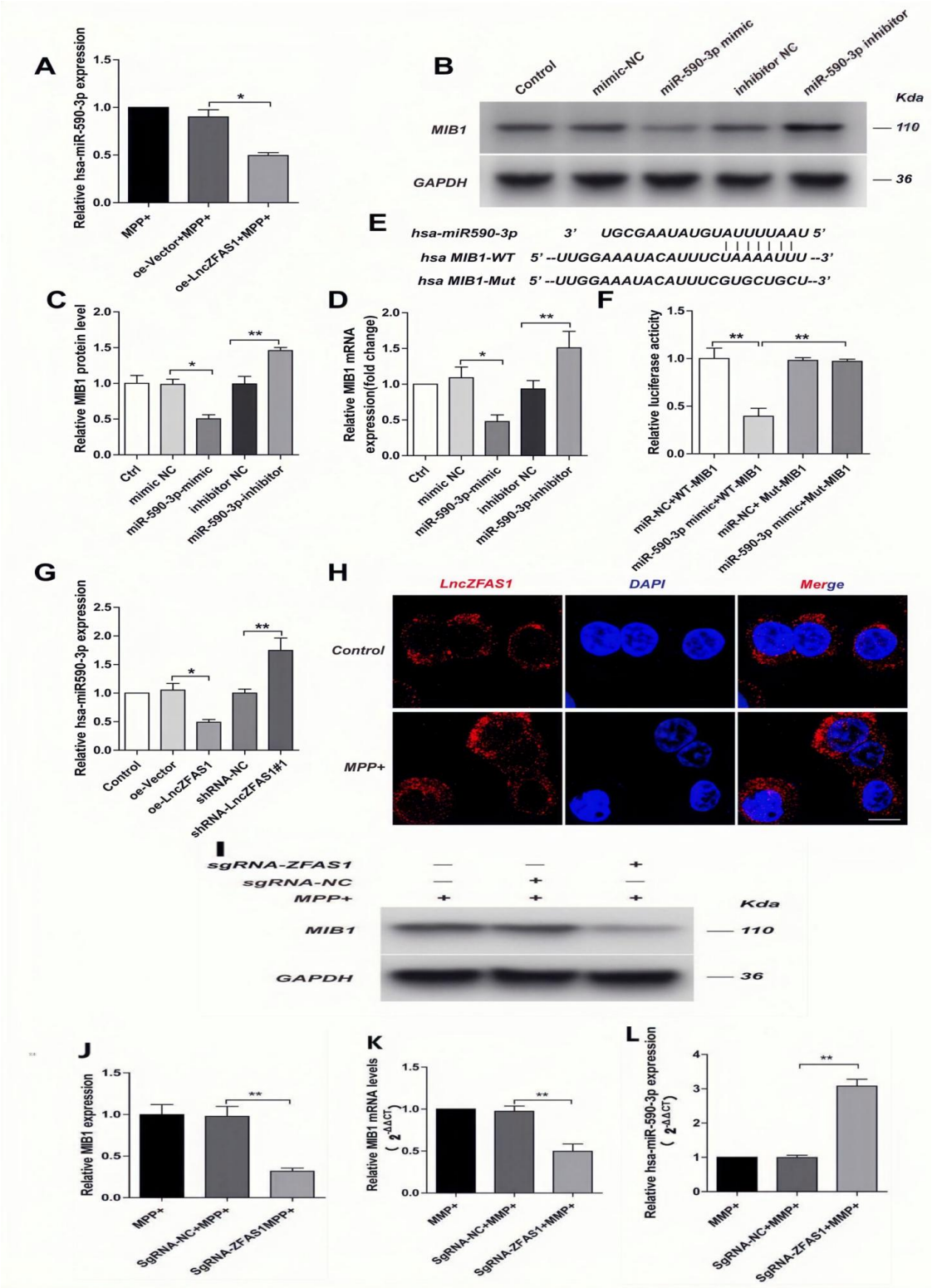

Figure 9

Fig. 9 LncZFAS1 regulates miR590-3p-mediated MIB-1 inhibition. SH-SY5Y cells were stably transfected with lentiviral vector for LncZFAS1 over expression or corresponding empty vector control, treated with MPP+ (1 mM) for 24h and Mir590-3p transcriptional levels were measure by qRT-PCR (A). Sh-SY5Y cells were treated with miR590-3p mimic, miR590-inhibitor or corresponding controls, and MIB1 levels measure by western blot (B, C) or qRT-PCR (D). A MIB1 luciferase reporter system was generated and the miR-590-

3p 3'UTR target sequence mutated for resistance (E). Transfected cells were treated with miR590-3p mimic, miR590-inhibitor or corresponding controls and MIB1 levels measured by luciferase activity (F). SH-SY5Y cells were stably transfected with lentiviral vector for LncZFAS1 over expression, ShRNA-ZFAS1 for LcnZFAS1 knockdown, or corresponding controls, and miR509-3p levels measured by qRT-PCR (G). SH-SY5Y cells were treated with MPP+ (1 mM) for 24h and LncZFAS1 intracellular localization determined by FISH staining and confocal microscopy. LncZFAS1 stably knockout SH-SY5Y cells (sgRNA-ZFAS1) were treated with MPP+ (1 mM) for 24h and MIB1 expression detected by western blot assay (I, J). MIB1 (K) and has-miR-590-3p (L) transcriptional levels were measured by qPCR. A, B and H results are representative of three independent experiments. C, D, F, G, J, K and L data represented as mean ± SD of three individual experiments for each condition, performed in triplicate. *p < 0.05, **p < 0.01.

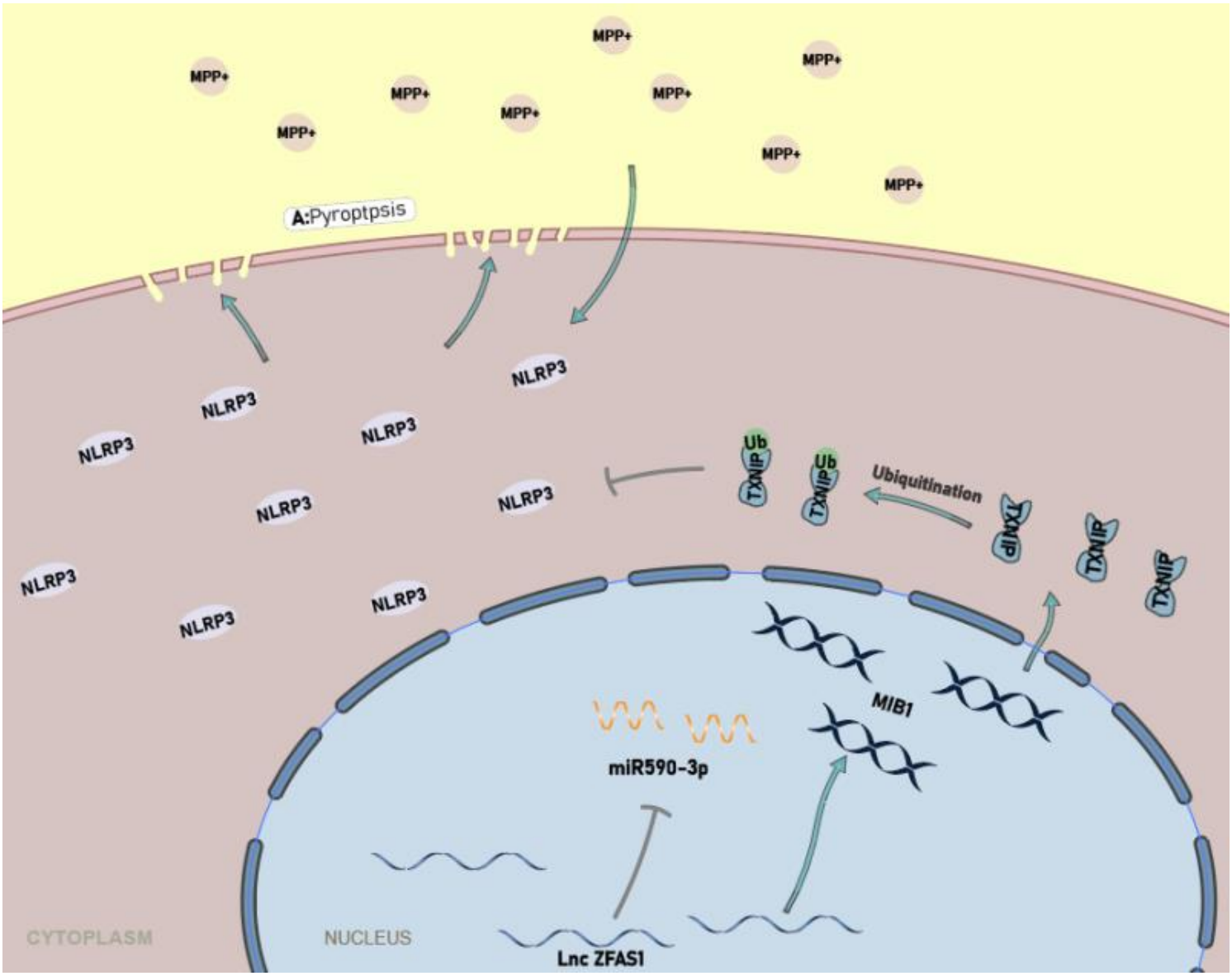

Figure 10

Fig. 10 Molecular mechanism for LncZFAS1 mediated inflammasome regulation in neuronal cells. Under homeostasis MIB1-mediated TXNIP ubiquitination inhibits inflammasome activation to maintain a

tolerogenic environment. Upon a Neuroinflammatory signal (MPP+) miR590-3p up-regulation inhibits MIB1 ubiquitin ligase, decreasing cytoplasmic Ub-TXNIP. In parallel, increased intracellular ROS activates the Txnip/TRX redox-sensing complex driving NLRP3/ASC association, leading to NLRP3 inflammasome activation and break of tolerance. lncZFAS up-regulation inhibits this entire pathway through direct interference with miR590-3p, preventing MIB1 ubiquitin ligase inhibition.

Supplementary Files

This is a list of supplementary files associated with this preprint. Click to download.

- Fig.S1.tif
- Fig.S2.tif
- Fig.S3.tif
- Fig.S4.tif
- formula.docx